Sedimentary Geology 316 (2015) 13–25

Contents lists available at ScienceDirect

Sedimentary Geology

journal homepage: www.elsevier.com/locate/sedgeo

# Compositional trends through the Holocene mud succession of the southwestern Black Sea shelf: Implications for sedimentary provenance and water-level history

Christopher J. Lister [a], Richard N. Hiscott [a,*], Ali E. Aksu [a], Peta J. Mudie [a,b]

[a] Earth Sciences Department, Memorial University of Newfoundland, St. John's, NL A1B 3X5, Canada
[b] Geological Survey of Canada-Atlantic, Box 1002, Dartmouth, NS B2Y 4A2, Canada

ARTICLE INFO

*Article history:*
Received 25 September 2014
Received in revised form 19 November 2014
Accepted 20 November 2014
Available online 27 November 2014

Editor: J. Knight

*Keywords:*
Provenance
Holocene
X-ray diffraction analysis
Clay minerals
Black Sea
Loess

ABSTRACT

Cores MAR02-45 and MAR05-03 were raised from 68–69 m water depth on the SW Black Sea shelf and indicate transgression and submergence beneath several tens of metres of water before 11.0 cal ka. Those who postulate a Black Sea lowstand below −100 m until the approximately 9.1 cal ka reconnection with the world ocean have suggested that sites like MAR02-45 and MAR05-03 must have been located in perched lakes on what is now the modern shelf. However, the silt- and clay-fraction mineralogy of samples from MAR02-45 provides no evidence for a shift in provenance at 9.1 cal ka, with earlier input from local rivers and later input from a broader region. Sedimentary abundances of Sc, Fe, Co, Ce, La, Th and Y also show no significant downcore trends. These elements likely reside in aluminosilicate mineral grains shed from terrestrial sources, so negligible downcore variation suggests long-term continuity in the composition of the detrital supply. More critically, the volume of pre-9.1 cal ka sediment around the MAR02-45 and MAR05-03 sites is >25 times the expected yield from local rivers over a 5000 year period, so other more substantial sources are required. The predominant silt size of the recovered sediments, the configuration of late Holocene currents in the western Black Sea, and analogies with dispersal systems elsewhere suggest that the bulk of the fine-grained muds at these sites likely came from the Danube and Kamchiya drainage basins where thick deposits of unconsolidated Pleistocene loess have been strongly dissected. To reach core sites on the SW Black Sea shelf, this material must have been advected from the Danube and Kamchiya deltas by unobstructed marine currents. Only thin event beds (tempestites) of fine sand and silt in the lower part of cores MAR02-45 and MAR05-03 are interpreted to have a local source in the Strandja Mountains of Thrace. Comparison of the palynology of surface samples from the Danube Delta and its associated coastal lagoons with the pre-9.1 cal ka sediments of core MAR02-45 confirms that the hypothesis of deposition in a perched ancient lake is untenable.



## 1. Introduction

Almost two decades have passed since the proposal by Ryan et al. (1997) and Ryan and Pitman (1999) that the Black Sea was catastrophically inundated by Mediterranean waters when global sea level rose above the floor of the Bosphorus Strait (~ −40 m elevation 'relative to modern sea level', hereafter rmsl). This proposed flooding event is most recently dated by Ryan et al. (2003) at 8400 conventional radiocarbon years before present ($^{14}$C yr BP; uncalibrated to calendar years and with no marine reservoir correction), equivalent to ~9.1 cal ka using the Marine09 calibration curve and $\Delta R = -105$ years (reservoir age ~300 years) consistent with Soulet et al. (2011) and Mertens et al.(2012). Immediately prior to the inundation, adherants to the scenario of a catastrophic flood propose that the level of the Black Sea was below −100 m rmsl (Ballard et al., 2000; Ryan et al., 2003; Lericolais et al., 2007; Nicholas et al., 2011), implying a large deficit of river runoff and precipitation relative to evaporation, unlike today (Özsoy et al., 1995).

Other researchers have argued that the pre-reconnection level of the Black Sea was near or above the level of the floor of the Bosphorus Strait by the time that the first Mediterranean waters penetrated into the Black Sea (Hiscott et al., 2007a, 2007b; Yanko-Hombach, 2007; Giosan et al., 2009; Yanko-Hombach et al., 2013; Mudie et al., 2014). A critical piston core that has provided support for this view is MAR02-45, raised from a water depth of −69 m rmsl on the southwestern Black Sea shelf near the border between Turkey and Bulgaria (41° 41.17′N, 28° 19.08′E; Fig. 1). This core is 9.5 m long with a continuous, high-resolution sedimentary record in its lower 6.8 m, spanning 10.3–5.5 cal ka (Mertens et al., 2012) and, thus, the entire time of the reconnection between the Black Sea and the world ocean. In many other parts of the

* Corresponding author. Tel.: +1 709 5791932.
*E-mail addresses:* chrisjlister@gmail.com (C.J. Lister), rhiscott@mun.ca (R.N. Hiscott), aaksu@mun.ca (A.E. Aksu), Peta.Mudie@NRCan-RNCan.gc.ca (P.J. Mudie).

http://dx.doi.org/10.1016/j.sedgeo.2014.11.004
0037-0738/

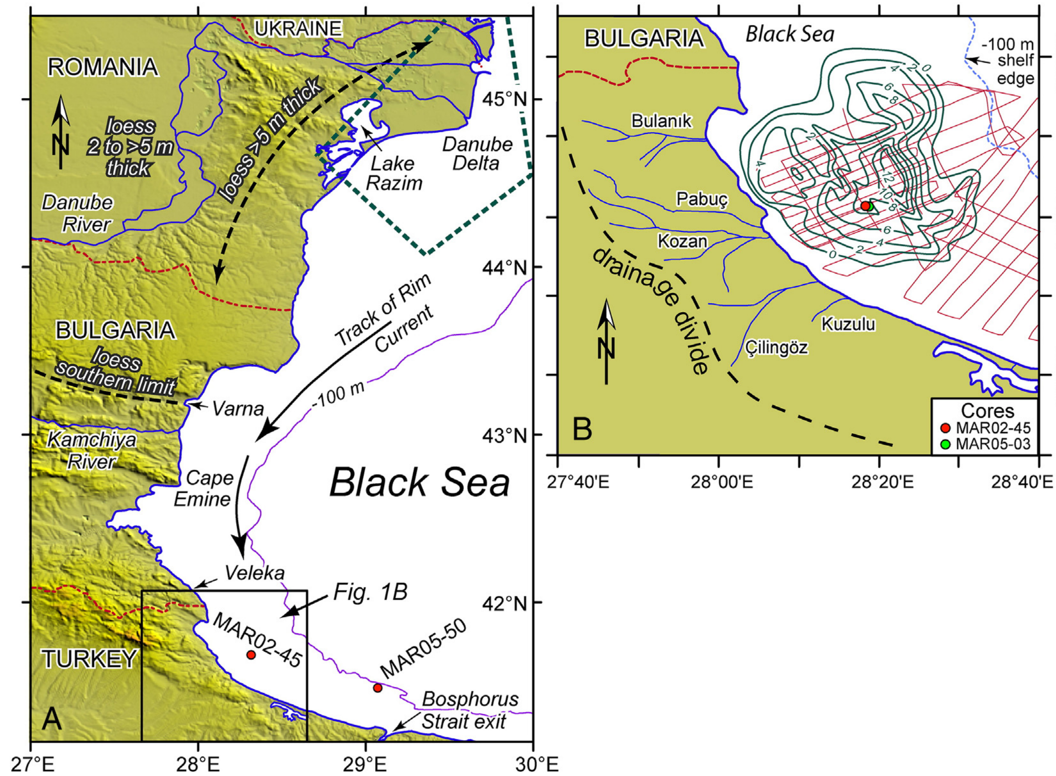


**Fig. 1.** (A) Location map of western Black Sea extending from Danube Delta to Bosphorus Strait. Sun-shaded topography of land areas from Ryan et al. (2009). Loess thicknesses and approximate southern limit from Haase et al. (2007). Lower box shows location of part B. Upper dashed polygon encloses palynology sampling sites of Frail-Gauthier and Mudie (2014) around the Danube Delta. North arrow is 50 km long. (B) Location map showing seismic tracks (i.e., the grid of mostly parallel lines) around the MAR02-45 and MAR05-03 core sites. Isopach contours (in milliseconds of two-way travel time) for seismic unit 1B (equivalent to lithologic Unit C of Hiscott et al., 2007a) were determined from seismic profiles, except northwest of the seismic grid where contours were closed in a conservative manner consistent with the shape of the main "bulls-eye" near the core sites. The contours were closed to enable volume calculation; the conservative extrapolation shown here minimizes the calculated volume of seismic unit 1B on this part of the shelf. Also shown are local small rivers north of the drainage divide (Okay and Okay, 2002) in the Strandja Mountains of NW Thrace. North arrow is 20 km long.

southwestern shelf, there is a subtle erosional unconformity called α1 (Aksu et al., 2002) which, ~5.25 m below the seafloor (mbsf) at the MAR02-45 site (Hiscott et al., 2007a; Fig. 2A), flattens around this core site into a conformable surface with age ~8.0 cal ka. The α1 level separates lowermost lithologic Unit C in the core from Unit B. A second, shallower unconformity (α2 of Aksu et al., 2002) is present 2.70 mbsf at the MAR02-45 site (Fig. 2A), and represents a hiatus from 2050–5465 cal yr BP (Mertens et al., 2012). α2 defines the top of lithologic Unit B and the base of the uppermost Unit A (Hiscott et al., 2007a). α2, and α1 where it is an unconformity, are both interpreted as submarine erosional surfaces that formed beneath strong shelf currents, presumably when sediment supply was insufficient to maintain accumulation. A comparable and analogous modern erosional surface has developed on a portion of the seabed north of the Bosphorus Strait (Flood et al., 2009).

Unit A is comprised of subtly colour-banded bioturbated silty mud with silt laminae and several molluscs of Mediterranean affinity. Unit B consists of alternating beds of silty mud and shelly mud. Molluscs (e.g., *Truncatella subcylindrica*, *Mytilus galloprovincialis*, *Parvicardium exiguum*) and bioclastic sand locally exceed 20 wt.% (Fig. 2B). Unit C consists of burrowed silty mud with graded beds of silt and fine sand. Molluscs include *T. subcylindrica*, *Monodacna pontica*, *Didacna* spp., *Dreissena polymorpha* and *D. rostiformis* (Hiscott et al., 2007a, 2010). In pre-reconnection (older than 9.1 cal ka) sediments of Unit C, the presence of thin beds of silt and very fine sand devoid of any evidence of wave reworking suggests that the water depth at the MAR02-45 site was of the order of some tens of metres (Hiscott et al., 2007a), and therefore the elevation of the local sea surface could not have been below approximately −40 m to −50 m rmsl (calculated, in metres, as −69-9.5 + [30 to 40]).

A second piston core, MAR05-03 (41°40.92′N, 28°18.99′E), was collected within ~500 m of the MAR02-45 site in an attempt to reach the transgressive unconformity, α (Aksu et al., 2002). Because the strata in this area have little dip or lateral thickness change (Hiscott and Aksu, 2002, their Fig. 16), the age–depth curve and facies of this core closely match the middle to lower Holocene stratigraphy of core MAR02-45, but the recovery extends ~75 cm deeper to 10.2 m below the seafloor (mbsf) and reaches gravel draping the α unconformity. A *Dreissena* sp. shell 5 cm from the base of core MAR05-03 and immediately above the basal muddy gravel is dated to 11.9 cal ka (Reynolds, 2012), constraining the start of the transgression across this portion of the modern shelf.

If the pre-9.1 cal ka Black Sea had an elevation below −100 m rmsl (Ballard et al., 2000; Ryan et al., 2003; Lericolais et al., 2007; Nicholas et al., 2011), then the water covering the MAR02-45 and MAR05-03 sites could have been tens of metres deep only if the sites were isolated in a perched lagoon or lake on what is now the modern shelf. This possibility has been suggested by Ryan (2007) for shallow-water sites in the Sea of Azov and on the Romanian shelf which have yielded pre-9.1 cal ka dates; he has interpreted these settings as "saline ponds or limans that were located landward of the shoreline of the Neoeuxinian lake" (Ryan, 2007, p. 72). The term 'liman' is used in the Black Sea area for isolated to semi-isolated water bodies (lakes and lagoons) in the coastal zone, usually in the vicinity of river deltas (Shuisky, 1982). Sediment supply to a perched coastal lake, higher in its level than the nearby receiving basin, can only come from local watersheds, implying a local bedrock provenance and a deposit volume controlled by the sediment yields of streams entering the lake. On the Turkish coast adjacent to the MAR02-45 and MAR05-03 sites, there are five small rivers and streams that might account for such local sediment supply (Aksu

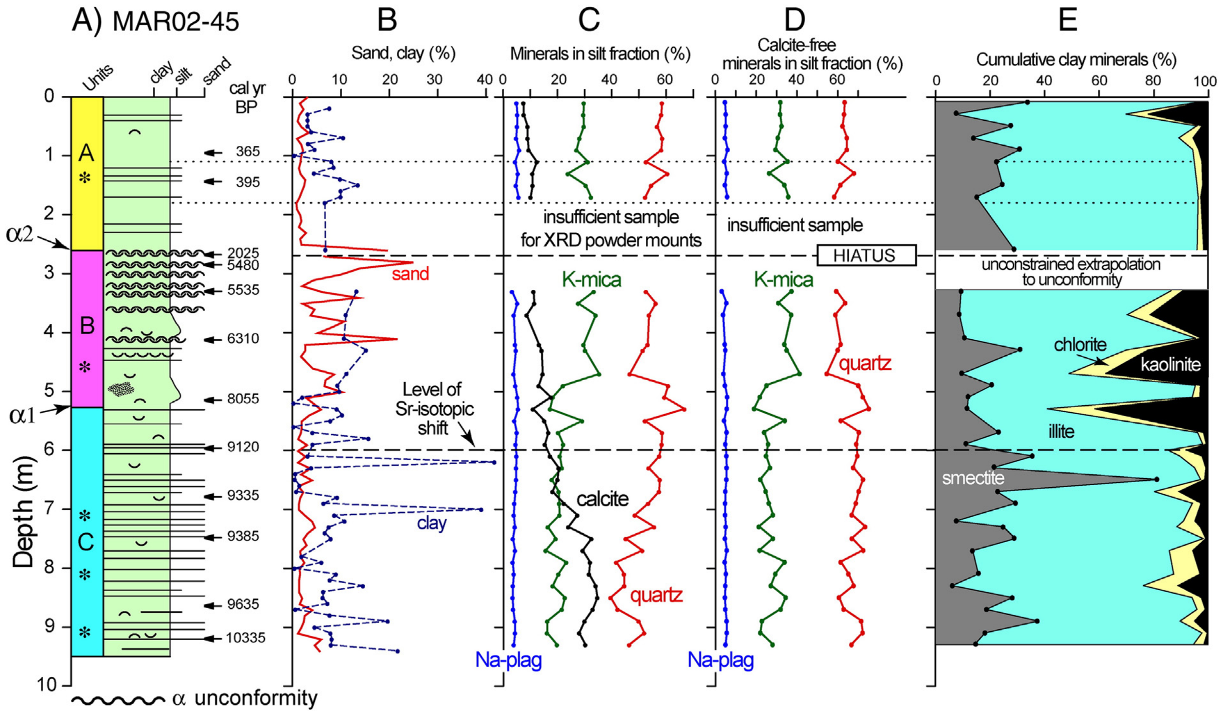


**Fig. 2.** (A) Sedimentary profile for core MAR02-45, from Hiscott et al. (2007a) who also present the downcore variation of total organic carbon, sulphur, their stable isotopes, and several faunal and floral genera. Calibrated radiocarbon dates from Mertens et al. (2012). Depth to transgressive unconformity, α, from Reynolds (2012). Asterisks mark depths of smear slides used to assess the origin of calcite. (B) Proportions of sand (from Hiscott et al., 2007a) and clay (from Lister, 2014); the remainder – silt – is generally >80%. (C) Minerals in the silt fraction of samples, recalculated to 100%, hence ignoring minor minerals (<5%) undetected by JADE® software. Data gaps result from insufficient sample at some depths for XRD analysis. (D) Silicate minerals in the silt fraction of samples, recalculated to 100% without calcite. (E) Proportions of the major clay minerals in <2 μm fractions, obtained using Biscaye (1965) weighting factors and recalculation to 100%.

et al., 2002). Today, these have a combined annual sediment yield of ~30,000 tonnes (EIE, 1991; Aksu et al., 2002).

As a contribution to clarifying the Holocene water level of the Black Sea prior to its reconnection to the world ocean, 1120 line-km of seismic profiles around the MAR02-45 and MAR05-03 sites (Fig. 1) and samples from core MAR02-45 were studied to ascertain the likelihood of pre-9.1 cal ka deposition in an isolated coastal lake. The characteristics of surface samples from the Danube and Dneister deltas, studied by Frail-Gauthier and Mudie (2014) for possible palynological analogs of paleo-liman depositional environments, contribute to the interpretations of this paper. The contrary hypothesis to accumulation in a coastal lake is that the MAR02-45 and MAR05-03 sites were open to the main Black Sea basin since the shelf was transgressed at ~11–12 cal ka (Aksu et al., 2002; Reynolds, 2012), and that the level of the Black Sea was much higher than −100 m rmsl at that time and since.

Our study of Black Sea water level in the early Holocene contributes to three issues of global interest. (1) Linkage between the Black Sea and Mediterranean Sea determines the importance of the Black Sea as a carbon sink and potential methane source of significant size in the global budget (Riedinger et al., 2010). The Holocene connection of these water bodies created a strongly stratified Black Sea, making it Earth's largest anoxic basin and a major carbon sink. Without connection, the basinal water would have remained oxygenated. (2) Measurement of the rates of major geomorphological changes in the Black Sea basin is crucial for understanding the spread of Neolithic human cultures and agricultural technology from Asia to central and western Europe (Carozza et al., 2012). In particular, detailed knowledge of how the Black Sea coast and paleo-deltas changed with sea level rise is necessary for determining how humans adapted to rapid landscape changes. (3) Climate shifts over Eurasia and the level of the global ocean modulate freshwater and saltwater inputs to the Black Sea and regulate its surface area, which is of hemispheric climatic importance (Coolen et al., 2013). The likelihood of Pre-Boreal (~11.6–9 cal ka) climate conditions dry enough to sustain a low Black Sea shoreline (and therefore a relatively small surface area) versus the likelihood that the early Holocene water body had a large surface area (because of early transgression) is still debated by geoscientists working in the region. This paper contributes to that debate.

## 2. Methods

Samples taken at 20 cm intervals throughout the core MAR02-45 were separated into sand, silt and clay fractions by wet sieving to separate sand and then settling, under tranquil conditions, of a suspension dispersed in 0.05% Na-hexametaphosphate (calgon) (Lister, 2014). This core had previously been extensively sampled for other work (Evans, 2004; Hiscott et al., 2007a; Marret et al., 2009), so at some sample depths, mostly just above and below the α2 unconformity, there was insufficient material for mineralogical analyses. However, there are no gaps in the sampling near the time of the reconnection between the Black Sea and the world ocean.

Where material was sufficient, the silt fraction was powdered, spiked with 5% molybdenite as an internal standard (Quakernaat, 1970), gently packed into special holders to create unoriented mounts ~2 mm thick for X-ray diffraction (XRD) analysis, and scanned using a Rigaku Ultima IV diffractometer, Cu-Kα radiation, a beam current of 40 kV at 44 mA, a divergent slit of 10 mm, a receiving slit of 0.3 mm and a scan speed of 1° min$^{-1}$ for most runs. Samples were scanned from 5–40° 2θ with a step size of 0.02° 2θ. Mineralogical analysis was done using JADE® software with whole pattern fitting in order to determine the weight percentage of constitutents using a cubic spline to resolve peaks from the background. This software only identifies minerals comprising at least 5% of the sample. The final JADE® output totals 100%, so the presence of minor amounts of unidentified (and unquantified) minerals inevitably results in a slight overestimation of the abundances of the identified mineral species. With no undetected minerals present in test mixtures of pure minerals, the accuracy achieved by JADE® is ±5% of the true abundances.

Clay fractions were spiked with 5% molybdenite, and mixed into a homogeneous paste with sparse amounts of a 0.2 M solution of $MgCl_2$. This paste was then smeared onto an acrylic slide using the thin edge of a piece of photographic film (Gibbs, 1965). Oriented clay mounts were run three times using the Rigaku Ultima IV diffractometer: once 'glycolated' and twice 'air dried'. The glycolated analyses were performed after the samples had been exposed to ethylene glycol for at least 8 h at ~60 °C; in this case, the diffractometer scanned between 5 and 17° 2θ. The first 'air-dried' scan provided data from 5–40° 2θ using a speed of 1° 2θ $min^{-1}$ and a step size of 0.02° 2θ. The second run focused on the 25–28° 2θ range and scanned using a step size of 0.005° 2θ to resolve the areas of partly overlapping chlorite and kaolinite peaks (Biscaye, 1964). Spectra for runs on clay minerals were analysed using MacDiff freeware (Petschick, 2000) to determine the areas of diagnostic mineral peaks in the <2 μm fraction after fitting a background baseline. JADE® software was not used to analyse data for oriented mounts because that software only identifies a mineral if the XRD spectrum contains all diagnostic peaks for the particular mineral, with the relative intensities of the peaks matching those in the proprietary mineral database. This is not the case for XRD scans of oriented phyllosilicate minerals, because non-basal reflections are suppressed or absent.

Spectra from the three separate runs on oriented clay mounts were aligned, scaled to one another, and corrected for 'displacement errors' (Pérez-Arrieta and Tabares-Muñoz, 2002) using the position and area of the 0.615 nm molybdenite peak. Diagnostic peaks for minerals identified in the clay-sized fractions are: smectite, 1.7 nm after glycolation; illite, 1.0 nm; chlorite, 0.7 nm; kaolinite, 0.7 nm; quartz, 0.4257 nm; calcite, 0.3034 nm; dolomite, 0.288 nm. Mixed-layer clays were not identified. Approximately 10% of the samples had too little clay to prepare oriented mounts, and downcore plots reflect this. In some cases, the overlapping chlorite and kaolinite peaks were too weak for trustworthy deconvolution, and in those cases the apportionment of the 0.7 nm peak was based on results from adjacent samples.

The relative proportions of minerals in each <2 μm sample were obtained in an iterative fashion (details in Lister, 2014), and then at the very end were recalculated to 100%. First, the proportion of quartz relative to total clay minerals was quantified using normalization factors of Underwood et al. (2003, their Table 4). For reasons explained below, the individual clay mineral proportions obtained using the Underwood et al. (2003) factors were not retained, and instead the relative amounts of smectite, illite, kaolinite and chlorite were obtained from their characteristic peak areas and the factors of Biscaye (1965), followed by scaling of their total to match the previously quantified total clay abundance. The amount of calcite relative to the amount of quartz was quantified using a relationship (Eq. 1) derived from data for these minerals in unoriented powder mounts (Underwood et al., 2003, their Table 3), based on an assumption that the relative peak areas of nonplaty quartz and calcite should be the same in both oriented and unoriented preparations.

$$\frac{\text{quartz}\ \ wt\%}{\text{calcite}\ \ wt\%} = 1.2723 \times \frac{\text{quartz}\ \ 0.4257\,\text{nm}\ \ \text{peak}\ \ \text{area}}{\text{calcite}\ \ 0.3034\,\text{nm}\ \ \text{peak}\ \ \text{area}} \tag{1}$$

Finally, the relative proportion of dolomite to calcite was quantified using their peak intensities (Royse et al., 1971).

Initially, an attempt was made to apply the individual quantification factors of Underwood et al. (2003) to obtain abundances of smectite, illite and chlorite. The result was a significant number of small negative abundances for chlorite, and smectite estimates ~20% higher (as a percentage of clay minerals) than abundances determined using Biscaye (1965) scaling factors. A linear regression between smectite assessed in MAR02-45 samples using the two scaling procedures yields the relationship $y = 0.9753x - 20.65$, where $y$ = smectite as a percentage of clay minerals using Biscaye (1965) factors, and $x$ = smectite percentage using Underwood et al. (2003) factors. $x$ and $y$ are strongly correlated, with $R^2 = 0.872$. Underwood et al. (2003) advise that their factors are only valid for the mineral compositions, diffractometer, and instrument settings which they employed. The Memorial University instrument uses different slit sizes and current, and it is unlikely that the Black Sea clay minerals are identical to the Underwood et al. (2003) standard minerals. The ~20% discrepancy in estimates for smectite abundance induced the authors to look at other clay mineral data sets for sites in the western Black Sea (Table 1). These were all quantified using Biscaye (1965) factors. It is clear that estimates of smectite abundance are only similar to the values in this paper if Biscaye (1965) factors are used for the MAR02-45 data. Since the primary use of the MAR02-45 results is to assess stratigraphic variability and similarity to other published work, it was decided to use the same factors preferred by other Black Sea workers. Even if the clay mineral abundances reported in this paper are not strictly accurate, they are internally consistent and suitable for the determination of temporal changes in composition at the MAR02-45 site.

The same XRD techniques were applied to the silt and clay fractions of five samples from shallow embayments and channels on the top of the Danube Delta (water depths <12 m; 45° 9.535′N, 29° 38.341′E; 44° 56.949′N, 29° 30.200′E; 44° 53.779′N, 29° 34.902′E; 45° 24.509′N, 29° 32.658′E; 45° 23.166′N, 29° 35.411′E). Four additional samples were collected from the banks of local small rivers on the Turkish coast adjacent to the MAR02-45 and MAR05-03 sites, but these proved to be too sandy for clay-mineral studies and so are not discussed in this paper. Because of damming of these small rivers, there are no deltas to act as repositories for finer detritus.

A commercial laboratory (Activation Laboratories, Ancaster, Ontario, Canada) was used for geochemical analysis of powdered <63 μm samples taken each 10 cm in core MAR02-45 (thus at twice the frequency of the XRD sampling), and from the five sites on the Danube Delta. The Activation Laboratories four-acid digestion procedure, employing inductively coupled plasma optical emission spectroscopy (ICP-OES) and instrumental neutron activation (INAA), is designed to provide data on six major elements, four minor elements, twenty-nine trace elements and ten rare-earth elements. Detection limits are available from laboratory on-line documentation (Actlabs, 2010). The acid extractions for Al and S are partial, so results for those elements are not used here. Fourteen elements (Au, Ag, Cd, Mo, Be, Bi, Br, Hg, Ir, Se, Ta, W, Sn and Tb) had multiple samples below detection limits and are eliminated from further consideration. Nine certified standards were analysed by ICP-OES, and two internal laboratory standards were analysed by INAA to confirm the accuracy of the geochemical data.

ICP-OES determinations were replicated four or six times for six MAR02-45 samples to assess precision, and two or three times for INAA determinations on the same six samples. Each replicate determination used a fresh aliquot of powder and independent processing. Four of the six replicated samples have six independent ICP-OES determinations (for the elements Cu, Pb, Ni, Zn, Ca, K, Mg, Mn, P, Sr, Ti, V, Y) and three independent INAA determinations (for As, Ba, Br, Co, Cr, Cs, Eu, Fe, Hf, Na, Rb, Sb, Sc, Ta, Th, U, La, Ce, Nd, Sm, Yb, Lu). For the ICP-OES determinations, precision is only considered acceptable if the sample standard deviation divided by the sample mean, averaged across the six samples, is <10% (hence uncertainty is <10% of the amount present). For several elements (Ni, Ca, Mg, Mn, Sr, V, Y) this statistic is <5%. For the INAA set of elements, reproducibility based on only three replications is harder to judge, and is calculated as ±1/2 the range for each set of replicates, divided by their average. Using this statistic, an uncertainty of <15% of the amount present is deemed acceptable, with the exception of Hf, U and Yb for which uncertainties of <20% of the amount present are accepted because the numerical values are generally <5 ppm, so small differences result in rather large percentage discrepancies from one run to the next. Twenty-four elements were judged to have acceptable precision: Na, Mg, K, Ca, Sc, V, Cr, Mn, Fe, Co, Ni, Cu,

**Table 1**
Percentages of clay minerals in Holocene sediments of the western Black Sea, estimated from downcore plots in the listed sources. Clay minerals are scaled to 100%. The Bayhan et al. (2005) gravity cores only sample the middle to late Holocene.

| Source | Core(s) | Position | Water depth | Size | Normalization | Smectite | Illite | Chlorite | Kaolinite |
|---|---|---|---|---|---|---|---|---|---|
| Bayhan et al. (2005) | GBK12, GBK13 | 41.6125°N, 28.22167°E; 41.72000°N, 28.10333°E | ~50 m | <2 μm | Biscaye (1965) | 25–30 | 40–50 | 15–20 | 5–10 |
| Major et al. (2002) | BLKS9810 | 44.0673°N, 30.8447°E | 378 m | <2 μm | Biscaye (1965) | 5–10 | 50–55 | 20–25 | ~20 |
| Stoffers and Müller (1978) | DSDP 380 | 42.0090°N, 29.6137°E | 2107 m | <2 μm | Biscaye (1965) | 20–30 | 50–60 | ~10 | ~10 |
| This paper | MAR02-45 | 41.6862°N, 28.3180°E | 69 m | <2 μm | Biscaye (1965) | 10–25 | 50–70 | 5–10 | 5–20 |

Zn, As, Sr, Y, La, Ce, Sm, Yb, Hf, Pb, Th, and U. For the six elements in this group determined by INAA (Co, Cr, Fe, Na, Sc, La), analysis of two laboratory standards during client runs demonstrated accuracy within 5% of the certified values for Fe, Na and Sc, and within 8% for Co and Cr. La was systematically overestimated by ~1.5 ppm (~10% of the certified values). Only ten elements analysed by ICP-OES had a concentration, in at least three certified standards, greater than half the minimum MAR02-45 concentration and less than twice the maximum. For these elements, accuracy based on 5–13 determinations is within 5% of certified values for Mg and Mn, within 10% for Sr, Ni, K and Cu, within ~12% for Zn, and within ~20% for Pb, V and Y. Y was systematically underestimated in the certified standards by ~3–8 ppm.

The pre-9.1 cal ka sediments around core sites MAR02-45 and MAR05-03 lie between the seismic marker α1 and the older transgressive surface (α unconformity of Aksu et al., 2002) on the southwestern Black Sea shelf, corresponding closely to seismic unit 1B of Aksu et al. (2002). Previously published isopach maps (Aksu et al., 2002; Hiscott et al., 2007a), contoured in milliseconds of two-way travel time as measured in high-resolution boomer and sparker profiles, were checked using Huntec deep-towed boomer profiles from cruises in 2002 and 2005, and then were analysed using ImageJ freeware (http://rsbweb.nih.gov/ij/) to determine the areas enclosed by different thickness contours. Travel times were converted to thicknesses using an acoustic velocity of 1500 m $s^{-1}$. Measured areas were multiplied by the contour interval, in metres, and reasonable porosity estimates of 60–70% to obtain the volume and mass of mineral solids in seismic unit 1B on the southwestern Black Sea shelf between longitudes 28° 00′E and 28° 35′E, and south of latitude 42° 20′N.

Measurements of the annual sediment discharges of local Turkish rivers (EIE, 1991) are compromised by the fact that these rivers have been dammed for several decades. It was therefore decided to use an empirical equation to estimate latest Quaternary yields before human impact on the environment. Without human impact or hinterland glaciers, and with a substrate of sedimentary rocks (Okay, 2008) and unconsolidated alluvium, the BQART equation (Syvitski and Milliman, 2007) is based entirely on measured or estimated riverine water discharge (EIE, 1991), drainage basin area (EIE, 1991), maximum drainage basin relief (captured from Google Earth® scenes), and average annual temperature (estimated to have been ~15 °C).

## 3. Results

### 3.1. Texture and mineralogy

All lithologic units in core MAR02-45 (Fig. 2A) are dominated by silt-sized detritus (Fig. 2B; average 88% silt) that consists predominantly of quartz, K-mica, calcite and sodic plagioclase (Fig. 2C). JADE® software does not identify minor minerals, having <5% abundance in XRD powder mounts, accounting for this limited list. There is an upward decline in calcite, an increase in K-mica from the top of lithologic Unit C into Units B and A, an upward increase in quartz, and an increase of sodic plagioclase in Unit A. Data recalculated to 100% without calcite (Fig. 2D) show that the relative proportions of silicate minerals vary little through the cored succession. In Unit C, the average calcite-free composition is 68.0 ± 4.1% quartz, 26.6 ± 4.4% K-mica, and 5.4 ± 0.4% sodic plagioclase. For comparison, the Danube Delta silt fraction contains 9.0 ± 0.8% calcite. On a calcite-free basis, the five samples from the Danube system average 59.7 ± 8.5% quartz, 29.7 ± 9.2% K-mica, 7.3 ± 2.6% sodic plagioclase, and 3.3 ± 4.2% dolomite.

There are seven key minerals (three non-clay and four phyllosilicate) in the <2 μm fraction of MAR02-45. The average abundances and standard deviations of these minerals are 12.2 ± 5.6% quartz, 26.4 ± 16.7% calcite, 6.3 ± 3.0% dolomite, 12.7 ± 10.4% smectite, 36.0 ± 12.0% illite, 3.2 ± 2.8% chlorite, and 3.2 ± 3.7% kaolinite. Hence, phyllosilicates only comprise ~55% of the <2 μm fraction. Average clay-sized quartz abundance increases from the base of Unit C (10.9%) through Unit B (13.7%) and into Unit A (14.1%). As in the silt-sized fraction, calcite abundance in the clay-sized fraction decreases from the base to the top of the core (Unit C, 34.9%; Unit B, 21.7%; Unit A, 10.0%) and the same is true for dolomite (Unit C, 7.5%; Unit B, 6.0%; Unit A, 3.7%). Because the data form a closed array totaling 100%, increases in the carbonate minerals automatically cause decreases in the total of the silicate minerals.

Illite is the dominant phyllosilicate mineral with a core average of 67.1 ± 14.3%. Smectite is the second most abundant mineral (21.7 ± 13.7%) while chlorite and kaolinite account for 5.8 ± 4.7% and 5.4 ± 5.7%, respectively. The within-unit variation in clay-mineral proportions is high (Fig. 2E), so although average values suggest stratigraphic trends, the high standard deviations rule out the demonstration of significant differences through the Holocene succession, other than some higher kaolinite abundances in the more sandy Unit B. For comparison, the Danube delta-top samples average 45.8% illite, 25.0% smectite, 1.3% chlorite, 1.8% kaolinite, 13.8% quartz, 8.9% calcite and 3.4% dolomite. If phyllosilicate minerals are recalculated to 100%, the proportions are 62.0% illite, 33.8% smectite, 1.8% chlorite, and 2.4% kaolinite. Both the MAR02-45 and Danube Delta results are broadly consistent with other published clay mineral proportions from the western Black Sea (Table 1).

### 3.2. Geochemistry

To assess relationships and trends in the geochemical dataset, correlation coefficients were calculated for those twenty-four elements having acceptable precision and abundances (relative to detection limits). This was done for the entire MAR02-45 succession, and then separately for lithologic units A, B and C (Fig. 3), omitting results for samples immediately adjacent to the α1 seismic marker (equivalent to an unconformity elsewhere on the shelf) and the α2 unconformity because of spikes in some elements at these levels (Lister, 2014). Since the 24 × 24 matrices are large, Fig. 3 only shows rows and columns for elements with at least one R value ≥ 0.8 or ≤ −0.8, indicating a strong relationship between that element and another in the matrix. These relationships are clearly shown in Venn-style diagrams (Fig. 4) like those used in set theory. Rings encircle elements with moderate (|R| ≥ 0.8) to strong (|R| ≥ 0.9) co-variation. Key elements (white font in Fig. 4) can be used as proxies for the behaviour of the other elements in each group. Hence, for the entire core, downcore plots of Ni, Zn, Th and Sc give a good summary of the trends for a wider range of elements (Fig. 5A). Considering all units, Sc, La and to a lesser extent Zn are useful guiding elements to understand cross-correlations. Ca invariably correlates with one or more of Mg, Sr and Mn, and tracks the abundance of calcite, as confirmed by a cross-plot (Fig. 6) of (a) Ca concentration in

All MAR02-45 samples

| | Cu | Pb | Ni | Zn | Ca | Co | Cr | Fe | K | Sc | Th | V | Ce | Sm | Yb |
|---|---|---|---|---|---|---|---|---|---|---|---|---|---|---|---|
| Cu | 1.00 | | | | | | | | | | | | | | |
| Pb | 0.70 | 1.00 | | | | | | | | | | | | | |
| Ni | ***0.82*** | ***0.81*** | 1.00 | | | | | | | | | | | | |
| Zn | ***0.86*** | ***0.86*** | ***0.93*** | 1.00 | | | | | | | | | | | |
| Ca | -0.57 | -0.67 | -0.69 | -0.77 | 1.00 | | | | | | | | | | |
| Co | 0.73 | 0.53 | 0.78 | 0.76 | -0.62 | 1.00 | | | | | | | | | |
| Cr | 0.58 | 0.34 | 0.63 | 0.57 | -0.47 | 0.78 | 1.00 | | | | | | | | |
| Fe | 0.73 | 0.49 | 0.79 | 0.77 | -0.65 | ***0.89*** | ***0.81*** | 1.00 | | | | | | | |
| K | 0.77 | 0.72 | ***0.90*** | ***0.89*** | -0.73 | 0.69 | 0.53 | 0.70 | 1.00 | | | | | | |
| Sc | 0.76 | 0.57 | ***0.81*** | ***0.82*** | -0.66 | ***0.89*** | 0.77 | ***0.93*** | 0.74 | 1.00 | | | | | |
| Th | 0.72 | 0.69 | ***0.83*** | ***0.83*** | ***-0.80*** | ***0.85*** | 0.72 | ***0.87*** | 0.75 | ***0.89*** | 1.00 | | | | |
| V | ***0.82*** | 0.74 | ***0.96*** | ***0.93*** | -0.71 | 0.78 | 0.60 | 0.78 | ***0.95*** | ***0.82*** | ***0.82*** | 1.00 | | | |
| Ce | 0.65 | 0.54 | 0.72 | 0.74 | ***-0.81*** | 0.79 | 0.73 | ***0.81*** | 0.70 | ***0.80*** | ***0.88*** | 0.74 | 1.00 | | |
| Sm | 0.42 | 0.44 | 0.44 | 0.50 | -0.59 | 0.59 | 0.47 | 0.60 | 0.40 | 0.71 | 0.78 | 0.47 | 0.62 | 1.00 | |
| Yb | 0.49 | 0.59 | 0.58 | 0.62 | -0.73 | 0.63 | 0.51 | 0.62 | 0.54 | 0.68 | ***0.85*** | 0.59 | 0.74 | ***0.87*** | 1.00 |

Unit A

| | Ca | Co | Fe | Mg | Sc | Sr | La | Sm |
|---|---|---|---|---|---|---|---|---|
| Ca | 1.00 | | | | | | | |
| Co | -0.55 | 1.00 | | | | | | |
| Fe | -0.53 | 0.72 | 1.00 | | | | | |
| Mg | ***0.91*** | -0.41 | -0.52 | 1.00 | | | | |
| Sc | -0.77 | ***0.80*** | ***0.83*** | -0.66 | 1.00 | | | |
| Sr | 0.73 | -0.34 | -0.42 | ***0.81*** | -0.43 | 1.00 | | |
| La | -0.65 | 0.49 | 0.64 | -0.66 | 0.75 | -0.54 | 1.00 | |
| Sm | -0.48 | 0.44 | 0.58 | -0.51 | 0.66 | -0.34 | ***0.93*** | 1.00 |

Unit C

| | Ni | Zn | Ca | Fe | K | Mn | Na | Sc | Sr | V | La | Sm |
|---|---|---|---|---|---|---|---|---|---|---|---|---|
| Ni | 1.00 | | | | | | | | | | | |
| Zn | 0.76 | 1.00 | | | | | | | | | | |
| Ca | 0.34 | -0.07 | 1.00 | | | | | | | | | |
| Fe | 0.79 | 0.68 | 0.27 | 1.00 | | | | | | | | |
| K | 0.72 | 0.78 | -0.31 | 0.54 | 1.00 | | | | | | | |
| Mn | 0.42 | 0.05 | ***0.80*** | 0.36 | -0.12 | 1.00 | | | | | | |
| Na | ***-0.81*** | -0.60 | -0.49 | -0.72 | -0.45 | -0.41 | 1.00 | | | | | |
| Sc | ***0.88*** | ***0.83*** | 0.10 | ***0.81*** | 0.79 | 0.18 | -0.77 | 1.00 | | | | |
| Sr | 0.43 | 0.03 | ***0.90*** | 0.30 | -0.13 | 0.65 | -0.51 | 0.19 | 1.00 | | | |
| V | ***0.91*** | ***0.85*** | 0.07 | 0.75 | ***0.89*** | 0.24 | -0.67 | ***0.89*** | 0.21 | 1.00 | | |
| La | -0.40 | -0.08 | -0.63 | -0.28 | 0.10 | -0.58 | 0.41 | -0.06 | -0.54 | -0.17 | 1.00 | |
| Sm | -0.42 | -0.06 | -0.64 | -0.29 | 0.11 | -0.56 | 0.44 | -0.10 | -0.52 | -0.15 | ***0.92*** | 1.00 |

Unit B

| | Cu | Ni | Zn | Ca | Co | Cr | Fe | K | Mn | Sc | Sr | Th | V | La | Sm | Yb |
|---|---|---|---|---|---|---|---|---|---|---|---|---|---|---|---|---|
| Cu | 1.00 | | | | | | | | | | | | | | | |
| Ni | 0.66 | 1.00 | | | | | | | | | | | | | | |
| Zn | ***0.88*** | ***0.85*** | 1.00 | | | | | | | | | | | | | |
| Ca | 0.04 | -0.08 | -0.03 | 1.00 | | | | | | | | | | | | |
| Co | 0.38 | 0.38 | 0.33 | 0.05 | 1.00 | | | | | | | | | | | |
| Cr | 0.24 | 0.41 | 0.32 | 0.05 | 0.78 | 1.00 | | | | | | | | | | |
| Fe | 0.36 | 0.37 | 0.33 | -0.25 | 0.70 | 0.78 | 1.00 | | | | | | | | | |
| K | 0.66 | ***0.82*** | ***0.86*** | 0.11 | 0.19 | 0.19 | 0.10 | 1.00 | | | | | | | | |
| Mn | 0.37 | 0.44 | 0.42 | 0.46 | 0.44 | 0.48 | 0.53 | 0.36 | 1.00 | | | | | | | |
| Sc | 0.38 | 0.40 | 0.38 | -0.14 | 0.73 | ***0.81*** | ***0.80*** | 0.12 | 0.50 | 1.00 | | | | | | |
| Sr | 0.11 | -0.01 | 0.00 | ***0.85*** | 0.03 | 0.11 | -0.04 | 0.06 | 0.46 | -0.10 | 1.00 | | | | | |
| Th | 0.25 | 0.38 | 0.26 | -0.05 | ***0.80*** | ***0.93*** | ***0.85*** | 0.08 | 0.50 | ***0.90*** | 0.01 | 1.00 | | | | |
| V | 0.72 | ***0.95*** | ***0.91*** | -0.05 | 0.35 | 0.39 | 0.29 | ***0.88*** | 0.39 | 0.39 | -0.04 | 0.33 | 1.00 | | | |
| La | 0.15 | 0.31 | 0.22 | -0.02 | 0.73 | ***0.93*** | 0.74 | 0.08 | 0.45 | ***0.85*** | 0.01 | ***0.95*** | 0.29 | 1.00 | | |
| Sm | 0.19 | 0.14 | 0.09 | -0.12 | 0.68 | 0.76 | 0.74 | -0.11 | 0.35 | ***0.92*** | -0.07 | ***0.88*** | 0.13 | ***0.84*** | 1.00 | |
| Yb | 0.15 | 0.23 | 0.13 | 0.02 | 0.77 | ***0.88*** | 0.76 | 0.02 | 0.46 | ***0.85*** | 0.06 | ***0.95*** | 0.22 | ***0.95*** | ***0.90*** | 1.00 |

**Fig. 3.** Partial matrices of correlation coefficients, R, reduced in size for publication by eliminating rows and columns for chemical elements having no cross-correlations with |R| ≥ 0.80. In remaining cells for the entire MAR03-45 core and separate lithologic units, stronger correlations are set in italics bold and highlighted. Depths 250–270 cm and 470–490 cm were not used to calculate correlation coefficients for separate units because of geochemical spikes close to α1 and α2 which mask otherwise good correlations (Lister, 2014).

the <63 μm fraction against (b) calcite weight percentage from XRD runs on silt from the same sampling depth. Using the relationship between Ca content and calcite percentages (Fig. 6), the downcore trends of key elements not strongly associated with carbonate minerals can be plotted on a calcite-free basis (Fig. 5B) to more clearly reveal the chemical characteristics of the silicate bedrock in the source area(s).

For the entire MAR02-45 succession (Fig. 4A), there are two main elemental associations with a high degree of cross-correlation at an R ≥ ~0.9 level: (a) V, Ni, Zn, K; (b) Sc, Th, Fe, Co. Other elements correlate preferentially with some members of these two groups; e.g., Cr and Yb with Fe, Sm and Cu with Th, and Pb with Ni and Zn. In Unit A (Fig. 4B), Sm and La are strongly correlated, as are elements typically found in carbonates (i.e., Ca, Mg, Sr). Sc is correlated with Fe and Co at the R ≥ 0.8 level. Compared with relationships for the entire core, the number of strongly correlated elements in Unit A is small. Relationships in Unit B are somewhat more complex (Fig. 4C). There are stand-alone elemental associations of (a) Ca with Sr, and (b) Zn with V, Ni, K and Cu. There is a larger cluster of cross-correlating elements centred around Th, La, Yb and Sc, with correlation of Cr, Co, Fe and Sm to different subsets of Th, La, Yb and Sc. In Unit C (Fig. 4D), the carbonate-controlled elemental

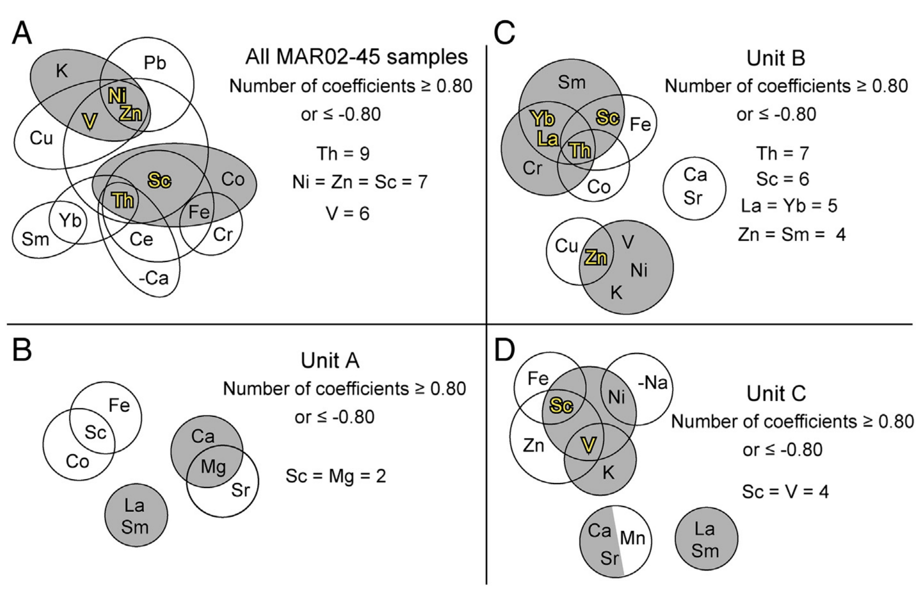


**Fig. 4.** Venn-style diagrams schematically expressing the relationships between elements from Fig. 3. The diagrams represent relationships throughout MAR02-45 and in the individual lithologic units. All elements within each ring have correlations to one another with |R| ≥ 0.80. Shaded areas show clusters of elements that mostly share correlations with |R| ≥ ~0.90. Within these shaded regions, the element(s) with the highest number of coefficients at the ≥ 0.80 level are in yellow outlined text (white in print version), and can be used as proxies for the behaviour of the other elements in the group.

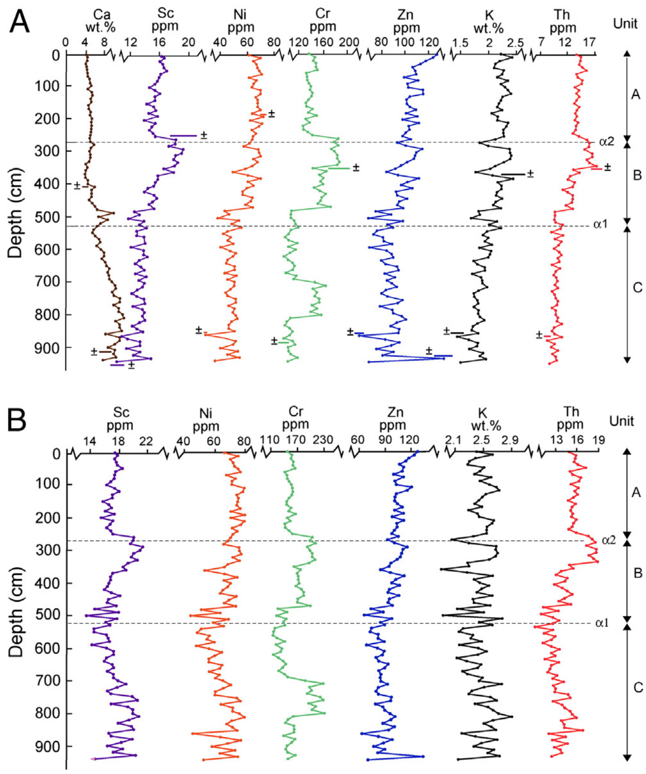

**Fig. 5.** (A) Downcore trends of those key elements in MAR02-45 that have strong cross-correlations throughout the cored succession (Figs. 3, 4). Below ~600 cm, dilution by calcite (tied to high Ca abundance) affects other downcore trends. Cr is included because it shows large shifts in abundance in Unit C. Uncertainty in the minimum and maximum value in each plot is shown as an error bar that is ± a percentage of the amount present, based on replicate analyses to quantify precision (Lister, 2014). (B) Downcore trends recalculated on a calcite-free basis using the linear relationship in Fig. 6. Ca is not included because it must drop to very low levels if calcite is ignored. Because calcite abundance might be overestimated in the silt-fraction XRD results by perhaps 10% of the amount present (see Fig. 6 caption), the elemental abundances shown here for the silicate fraction of Unit C are in reality slightly higher than shown, making some of the plots even more invariant with depth than shown (e.g., Ni, Zn).

association involves Ca, Sr and Mn. La and Sm are highly correlated to one another but to no other elements. The main cluster of cross-correlated elements hinges on a strong correlation of Sc, V, Ni and K,

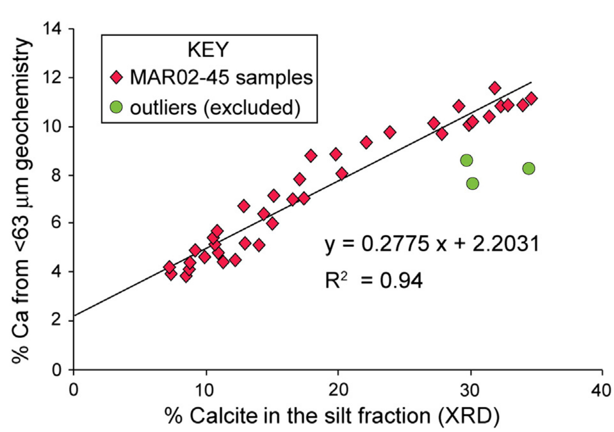


**Fig. 6.** Plot of percent Ca from geochemical analysis of <63 μm fractions versus calcite abundance determined by XRD analysis of the silt fractions of MAR02-45. The predominance of silt (Fig. 2B) validates this comparison, although the certain presence of other minerals at low abundance (<5%) in the silt fractions requires that the plotted calcite abundances are marginally overestimated — perhaps 10% higher than they should be. For example, a sample with 30% stoichiometric calcite should contain a minimum of 12% Ca, whereas the plotted results predict 30% calcite in samples with only 11% Ca. Implications are noted in the Fig. 5B caption. Three outliers that were excluded from the regression calculation are indicated by circles.

with additional correlation pairs (and one triplet): Sc and V with Zn; Fe with Sc; Ni with −Na (i.e., a negative correlation).

Because cross-correlations differ from unit to unit, the full geochemical dataset cannot be considered to have been drawn from a single multivariate population, as required for multivariate statistical techniques like principal component or factor analysis. Hence, this type of statistical analysis is not presented here.

### *3.3. Deposit volumes and sediment yields*

The total calculated volume of Holocene sediment in the region around core sites MAR02-45 and MAR05-03 (bounded by the landward zero thickness, the shelf edge, longitudes 28° 00′E and 28° 35′E, and latitude 42° 20′N) is 97.62 $km^3$. Seismic unit 1B (lithologic Unit C) accounts for 17.51 $km^3$ (Fig. 1B), seismic unit 1C (Unit B) for 24.92 $km^3$ and seismic unit 1D (Unit A) for 55.19 $km^3$. An interval of 5000 years was chosen as a reasonable duration for riverine input to seismic unit 1B (lithologic Unit C), allowing ~2000 years for the contribution after marine flooding, and ~3000 years for the prior deposition of subaerial floodplain deposits and deltaic deposits that might have been reworked into seismic unit 1B during the early Holocene transgression. Annual yield was calculated for the Bulanık, Pabuç, Kazan, Çilingöz and Kuzulu rivers using parameters explained in §2. The combined predicted annual yield is ~100,000 tonnes, or approximately three times the modern sediment discharge of the dammed rivers (EIE, 1991). If the yield from local rivers remained at this level for 5000 years, then a mass of 522.6 megatonnes of material could be expected from local river input. Marine muds have 60–70% porosity. At 60% porosity, the 522.6 megatonnes of mineral-density solids would occupy 40% of the sedimentary deposit. Using a mineral density of 2.65 tonnes/$m^3$, the equivalent volume of solids is 0.197 $km^3$, from which it follows that the volume of the sedimentary mass containing this amount of mineral solids and having 60% porosity would be $(100/40)(0.197) = 0.493$ $km^3$. Using 70% porosity, a similar calculation predicts 0.657 $km^3$ of porous mud over a 5000 year period. Even this larger volume is only ~4% of the measured volume of seismic unit 1B (lithologic Unit C).

## 4. Interpretation

There is an enormous discrepancy between the amount of lower Holocene sediment (Unit C) located on the southwestern Black Sea shelf (~17 $km^3$) and the volume of sediment potentially supplied by local rivers, as predicted by the BQART equation (~0.66 $km^3$, based on riverine supply for 5000 years). There are several ways to reconcile this discrepancy. The simplest approach would be to increase the timespan for the input from local sources; however, with all BQART parameters fixed, it would take ~250,000 years for local sources to supply 17 $km^3$ of sediment. Obviously this scenario is unrealistic, as basin parameters would have changed over that time (e.g., glacial-interglacial cycles), promoting removal to deeper water areas of most of the sediment as a consequence of erosion during lowstands and transgressive phases.

The BQART model is demonstrated to be accurate within a factor of 5× (Syvitski and Milliman, 2007), so at the upper limit the supply from local rivers over 5000 years might have been as high as 3.3 $km^3$. Using this maximum estimate, it would still take ~26,000 years for local watersheds to supply 17 $km^3$ of sediment.

A more plausible scenario involves contribution to Unit C from more distant sources. The Kamchiya Delta (Bulgaria) and the Danube Delta (Romania and Ukraine) are both significant sources of sediment to the west and north of core site MAR02-45. Distances from their deltas to the core site are ~130 km and ~380 km, respectively. During the early Holocene, flooding of the shelf caused the Danube River to cease direct supply to its deep-sea fan via the Viteaz Canyon (Popescu et al., 2001; Lericolais et al., 2012), instead building delta lobes mostly after ~9.5 cal ka (Panin et al., 1983) or after ~5.5 cal ka (Giosan et al., 2006). Today, there is strong southward advection of sediment along the shelf from the Danube Delta to Bulgarian and Turkish waters (Panin and Jipa, 2002), driven by longshore wind-driven currents and the geostrophic Rim Current (Oğuz and Beşiktepe, 1999) which tracks along the upper slope and shelf edge, interacting with non-stationary eddies near the shelf break (Ginzburg et al., 2002; Yankovsky et al., 2014).

Sediment discharge rates for the Kamchiya River (Jaoshvili, 2002) indicate a possible contribution to the shelf setting of ~7.1 $km^3$ of 70% porosity mud over 5000 years, a portion of which might have moved farther southeastward along the shelf. There are other smaller rivers along the Bulgarian and Romanian coastline that might have added some of their sediment load to the longshore current system and the counterclockwise-flowing Rim Current leading to the SW shelf (e.g., drainage into the Varna and Veleka estuaries and their adjacent shelf areas). In the vicinity of Cape Emine just downdrift of the Kamchiya Delta, the Holocene shelf succession reaches thicknesses of ~50 m (Dimitrov et al., 1998; Filipova-Marinova et al., 2004). This location is the usual terminus of the present-day migration of mesoscale slope eddies which entrain sediment from the Danube outflow (Ginzburg et al., 2002), but under some circumstances the eddies and low salinity water migrate further south, even beyond the Bosphorus Strait (Yankovsky et al., 2014). A significant contribution from river systems in general is supported by the preponderance of terrestrial organic carbon (Hiscott et al., 2007a) and the considerable amount of coarse plant debris, pollen and fern spores in palynology samples from Unit C in core MAR02-45. In addition, Unit C has relative abundances of aquatic pollen taxa, algal spores, *Pediastrum* ceonobia, and fungal remains (Table 2) which characterize modern sediments of the Danube delta front and prodelta (Hiscott et al., 2007a; Frail-Gauthier and Mudie, 2014). Along-shelf advection of sediment from major river deltas is able to provide significant material over distances greater than those noted above, for example up to 600–800 km from the mouths of Asian deltas (Liu et al., 2009).

During the latest Pleistocene lowstand of the Black Sea, the Danube River emptied directly into the Viteaz Canyon, feeding all of its suspended sediment to the Danube submarine fan (Winguth et al., 2000; Panin and Jipa, 2002; Popescu et al., 2004; Lericolais et al., 2012). The canyon heads in a water depth of −110 m and incises 26 km into the shelf edge (Popescu et al., 2004), but the shelf is ~140 km wide in this area, so with a sea-level rise to even the present −50 m bathymetric contour, the canyon would cease to capture the river sediment discharge. Today, the outer shelf is starved of terrigenous sediment (Panin and Jipa, 2002). According to Major et al. (2002), the decline in sediment supply to the slope adjacent to the upper Danube Fan occurred in two steps, at ~15 $^{14}$C ka and ~8.4 $^{14}$C ka (~9.1 cal ka). The more recent of these steps is associated with reconnection of the Black Sea to the global ocean. Major et al. (2002) estimated the time of the latest drop in accumulation rate by joining points on an age–depth curve for core BLKS9810, with the data points being uncalibrated conventional radiocarbon dates supplemented by an age of 8.4 $^{14}$C ka for the Sr-isotopic shift to open-ocean values and an age of 7.16 $^{14}$C ka widely accepted for the beginning of sapropel deposition in the deep basin (Fig. 7A). Instead, the authors believe it is more reasonable to use calendar ages, and to extrapolate neighbouring straight-line segments of approximately constant accumulation rate to a common intersection point (Fig. 7B). This is justified because the decline in sediment supply (presumably caused by transgression across the shelf) might have occurred any time between 9.1 cal ka and the next oldest calibrated date. This approach (Fig. 7B) predicts a significant sea-level rise and transgression by ~10.8 cal ka. Of course there are uncertainties associated with the original radiocarbon dates, marine reservoir ages, and calibration to calendar years. Nevertheless, the result is consistent with a switch from predominant sediment delivery to the deep basin (via the Viteaz Canyon) to sediment retention on the shelf by the onset of deposition of Unit C at core sites MAR02-45 and MAR05-3.

There are two other canyons in the northwestern Black Sea associated with the Dniester and Dnieper rivers. The Dnieper (or Dnepr) Canyon heads in ~70 m of water (Gulin et al., 2013) and so also would have ceased its capture of most of the river detrital supply after transgression to approximately the −50 m bathymetric contour. Because the Danube detrital load exceeds the Dniester and Dnieper loads by ~20–25 times (Panin and Jipa, 2002), the potential role of these more distant systems

**Table 2**
Summary of selected environmental parameters, palynological remains (from Frail-Gauthier and Mudie, 2014), and the dominant kerogen type(s) found in modern coastal freshwater limans, deltaic and shelf environments compared with results for lithologic Unit C in cores MAR02-45 and MAR05-50 (PJM previously unpublished data gathered using methods in Mudie et al., 2010).

| | Coastal region | | | | | | | | | | | | | | | | Lithologic unit C | |
|---|---|---|---|---|---|---|---|---|---|---|---|---|---|---|---|---|---|---|
| Environment[d] | Liman | Estuary | | L | L | L | D | D | D | P | P | P | P | S | S | S | MAR02-45 | MAR05-50 |
| Sample station[a] | Saskia | Chilia2 | St Georghe | R02 | R06 | R21 | 9 | 10 | 16 | 8 | 7 | 15 | 18 | 6 | 5 | 1 | 6 sample average | 8.3 mbsf |
| Depositional water depth (m) | 6 | 9 | 5 | 2.8 | 1.6 | 1.8 | 17.4 | 20.7 | 24.3 | 33.6 | 45.7 | 49.7 | 33.1 | 54.8 | 65.1 | 58.5 | 40–50 | 60–70 |
| Approximate distance from land (km) | 0 | 0 | 0 | 0 | 0 | 0 | 3 | 4 | 13 | 15 | 35 | 26 | 28 | 50 | 65 | 68 | 18 | 25 |
| Surface salinity during deposition | 2 | 2 | 2 | 1.8 | 2 | 2.04 | 5.5 | 5.7 | 7.6 | 10.4 | 13.6 | 7.6 | 16.6 | 15.5 | 16.5 | 16.1 | 14–15[b] | 14–15[b] |
| Kerogen type[c] | L | L | L | L | L | L+W | A | A | A | A | A | A+W | A | W | W | W+I | I | I |
| Pollen+spore (P+S) (% of total) | 49.0 | 44.9 | 49.4 | 61.1 | 59.2 | 50.0 | 60.5 | 50.0 | 60.9 | 43.7 | 32.8 | 41.1 | 58.8 | 26.5 | 34.8 | 25.0 | 87.0 | 52.5 |
| Aquatic (% of P+S) | 30.0 | 10.8 | 10.2 | 20.4 | 8.0 | 17.4 | 12.1 | 14.4 | 2.6 | 4.3 | 4.2 | 5.5 | 5.3 | 5.9 | 2.6 | 3.2 | 6.6 | 15.4 |
| Fern+moss (% of P+S) | 4.0 | 6.0 | 1.56 | 0 | 0.88 | 0 | 8.9 | 9.6 | 1.3 | 5.2 | 3.4 | 0 | 0 | 0.9 | 5.3 | 0 | 6.0 | 11.9 |
| Fungal (% of P+S) | 10.9 | 49.7 | 64.1 | 12.8 | 11.6 | 22.6 | 36.3 | 60.2 | 19.2 | 10.4 | 4.2 | 11.5 | 6.4 | 12.8 | 1.4 | 25.8 | 18.4 | 15.6 |
| Number *Glomus* (soil fungus) | *2* | 25 | 28 | 8 | 8 | 6 | 0 | 0 | 1 | 3 | 0 | 1 | 1 | 0 | 0 | 11 | 10 | 6 |
| Algal spores (% of total) | 15.0 | 5.0 | 8.1 | 4.9 | 9.3 | 6.5 | 2.4 | 6.0 | 4.4 | 9.5 | 4.9 | 7.8 | 9.5 | 9.1 | 7.9 | 6.8 | 2.9 | 9.3 |
| Number *Pediastrum* | 0 | 0 | 1 | 5 | 14 | 1 | 1 | 0 | 1 | 0 | 0 | 1 | 1 | 0 | 0 | 0 | 4 | 5 |
| Dinocysts (% of total) | 1.8 | 0.5 | 0 | 1.4 | 0.8 | 1.3 | 6.8 | 1.8 | 10.4 | 34.6 | 58.1 | 41.2 | 13.3 | 61.9 | 48 | 48.4 | 6.2 | 4.4 |
| Ratio pollen:dinocysts | 24.5 | 76.5 | 128 | 41.4 | 126.7 | 38.33 | 8.86 | 8.3 | 5.7 | 1.26 | 0.57 | 0.9 | 4.4 | 0.43 | 0.71 | 0.48 | 6.19 | 12.1 |
| Microfauna (% of total) | 25.5 | 11.2 | 10.8 | 17.7 | 23.8 | 27.2 | 3.5 | 6.4 | 10.2 | 7.6 | 2.8 | 9.8 | 13.2 | 6.3 | 6.4 | 8.5 | 10.7 | 16.8 |
| Insects (% of microfauna) | 18.5 | 9.5 | 7.1 | 3.7 | 2.4 | 3.3 | 0 | 0 | 0 | 5 | 0 | 8.3 | 0 | 3.6 | 4.8 | 4.8 | 1.9 | 11.1 |
| Number Thecamoebians | 1 | 7 | 3 | 0 | 0 | 0 | 1 | 0 | 0 | 6 | 3 | 3 | 0 | 0 | 1 | 1 | 0.5 | 0.0 |
| Number *Bosmina* (water flea) | 0 | 6 | 3 | 12 | 19 | 6 | 0 | 0 | 0 | 0 | 0 | 1 | 0 | 0 | 0 | 0 | 0.5 | 2 |
| Total palynomorphs | 106 | 372 | 259 | 345 | 380 | 230 | 205 | 166 | 248 | 263 | 362 | 486 | 158 | 441 | 327 | 248 | 241 | 160 |

[a] Danube Delta locations from Frail-Gauthier and Mudie (2014) and bracketed in Fig. 1A; Saskia Liman is in western Ukraine.
[b] Pre reconnection salinities from Mertens et al. (2012)
[c] Kerogen types: L=leaf; A=amorphous; I=indeterminate
[d] Column abbreviations are L = Lagoon, D = Delta front, P = Prodelta, S = Shelf.

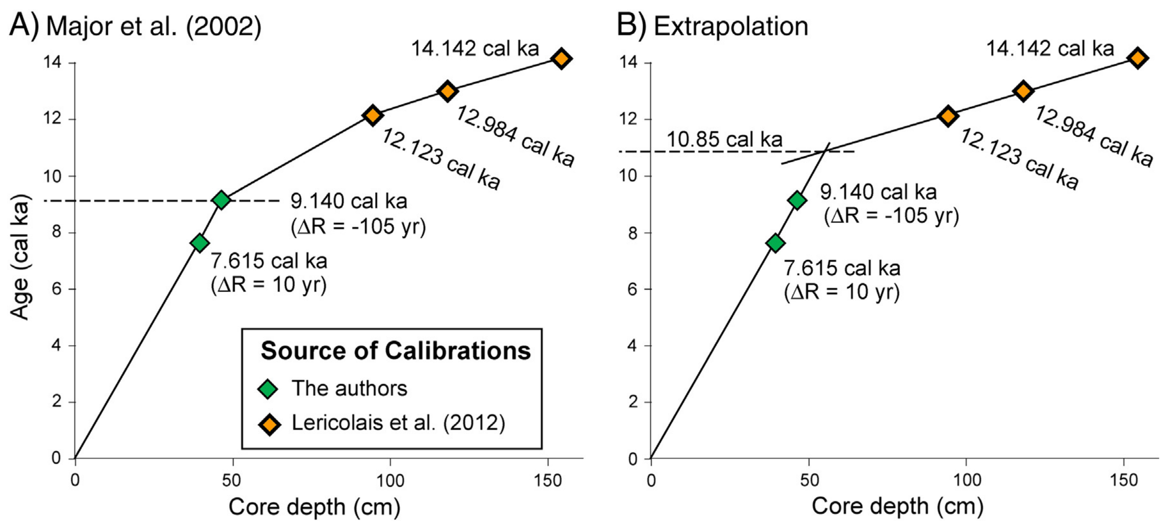


**Fig. 7.** Age–depth plots based on dated levels in core BLKS9810 (Major et al., 2002), calibrated to calendar years using the Marine09 curve and ΔR values of +10 years and −105 years (hence reservoir ages of ~415 yr and ~300 yr) for the youngest and next youngest dates, respectively, (consistent with Siani et al., 2000; Soulet et al., 2011) and calibrated dates extracted from Lericolais et al. (2012, their table 2) for older dates. Uncertainties are smaller than the size of the diamond-shaped symbols. (A) Age model consistent with the approach of Major et al. (2002), leading to a conclusion that the accumulation rate slowed at 9.14 cal ka, coincident with Sr-isotopic evidence for the incursion of Mediterranean seawater. (B) Age model based on extrapolation of two linear trends in accumulation rate to a common intersection point. The shift to a lower accumulation rate is calculated to have occurred at 10.85 cal ka, but if the decline was gradual over a number of centuries, then it might have started even earlier. The reduction in accumulation rate is inferred to coincide with a reduction in off-shelf sediment supply because of landward migration of the shoreline during earliest Holocene transgression.

in supplying sediment to the southwestern Black Sea is not considered further. There is, however, one age constraint from work on the shelf seaward of the Dneister Delta that should be noted here. Dated peats in that area suggest that the water level of the Black Sea was already at, or less than, about −40 m relative to the present by the time of the initial reconnection to the Mediterranean Sea, and benthic foraminifera and ostracods requiring 11–26 psu salinity indicate that this reconnection started ~8900 $^{14}$C yr BP (Yanko-Hombach et al., 2013; Mudie et al., 2014).

Is there reason to believe that southwardly directed along-shelf sediment transport immediately after the early Holocene transgression would have been comparable to the modern flux? Modern longshore transport on the western shelf is driven by prevailing winds from the NNE and ENE (Oğuz et al., 1995; Bayhan et al., 2005). The prevailing winds in the early Holocene likely were similar because of the influence of the large northern Eurasian land mass to the north of the Black Sea. Farther offshore, a precursor to the geostrophic Rim Current also likely existed. Oğuz et al. (1995) numerically modelled the first-order cyclonic circulation in the Black Sea, and found it to be governed by (a) wind stress, (b) density (thermohaline) contrasts created by evaporation–precipitation gradients and differential heating of the sea surface, and (c) buoyant riverine inflow from, principally, the Danube River. The Danube outflow turns preferentially to the right (i.e, the south) because of the Coriolis effect. In the early Holocene, the degree of stratification and the buoyant contrast between the fresh Danube outflow and the basinal water would have been less than today, but the Black Sea was never fresh, but rather had a pre-transgression salinity of ~14 psu (Mertens et al., 2012). Hence, buoyant characteristics of the Danube outflow and density contrasts caused by gradients in precipitation–evaporation and heat flux would have existed then as they do today. Furthermore, the earliest Holocene discharge of rivers entering the northwestern Black Sea is believed to have been similar to today, or even slightly greater (Sidorchuk et al., 2011), promoting the type of strong cyclonic circulation that characterizes the modern Rim Current.

A third possible source for some portion of the 17 km$^3$ in Unit C is reworking of Pleistocene shelf deposits that were subaerially exposed on the coastal plain (now the modern shelf) during the early Holocene transgression. There are sparse, long-spined (indicative of relatively high salinity) specimens of the dinoflagellate *Lingulodinium machaerophorum* toward the base of core MAR02-45 (Mertens et al., 2012). The last time the Black Sea salinity was similar to today, in order to account for this long spine length, was in the period 126.5–121 cal ka (Shumilovskikh et al., 2013). There are also rare specimens of the palynomorph genera *Multiplicisphaeridium* and *Romanodinium* in Unit C, the former being common in Miocene successions in northwestern Turkey, and the latter in Pliocene deposits of Romania (Baltes, 1971). These occurrences might indicate derivation of a small portion of the lowest Holocene succession by erosion of local unconsolidated or weakly consolidated deposits during the Holocene transgression.

The interpretation favoured here is that the mud fractions present in seismic units 1B–1D (lithologic units C–A) entered the Black Sea from terrestrial sources either during the time of the earliest Holocene transgression, or somewhat earlier following the Last Glacial Maximum (LGM). This influx could not have been supplied by local small rivers, so must have come from elsewhere along the Black Sea coast where large rivers enter the basin.

There is very little clay-sized material in the MAR02-45 samples. This is consistent with the grain-size reported from core MAR05-50 which penetrated these same units 40 km to the east (Flood et al., 2009). This is unlike typical marine muds which contain moderate amounts of clay (Weaver, 1989). The texture is similar, however, to that of loess deposits (Varga, 2011), which are widespread in the Danube drainage basin (Smalley and Leach, 1978; Haase et al., 2007; Fitzsimmons et al., 2012). The loess deposits in the Danube drainage basin can have thicknesses >5 m, and are deeply dissected by tributaries to the Danube River, and by northern tributaries to the Kamchiya River (Fitzsimmons et al., 2012). The loess has an age <1000 ka, with substantial loess accumulation occurring during the LGM and Younger Dryas (Fitzsimmons et al., 2012). Erosional dissection has occurred since the LGM, feeding large quantities of sediment with the textural characteristics of loess into the Danube system, and onward to its delta on the Black Sea coast. The close textural similarity of the MAR05-50 muds to loess, the position of the MAR05-50 site downcurrent from the MAR02-45 and MAR05-03 sites, and the presence of the same stratigraphic units at the two sites (Hiscott et al., 2007a; Flood et al., 2009) raise the possibility that the primary source for significant amounts of the Unit C sediment might be reworked loess. A similar suite of diagnostic palynomorphs indicative of fluvial transport also characterize the Unit C sediments of MAR05-50; in addition, there are common remains of Cladocera (water fleas, e.g. *Bosmina*) which today dominate in a coastal lagoon Lake Razim, south of the Danube Delta. However, in modern samples from the Danube Delta front and prodelta, the dinoflagellate percentages typical of Unit C are only found in the delta front samples with surface salinity below 10 psu (Table 2).

Mineralogy of the silt fraction does not point to particular source areas, or to a changing provenance since the latest Pleistocene to early Holocene transgression began. There is an ~6% decrease in quartz and an increase in K-mica content (~5%) upwards through the core, but the large standard deviations for these components prevent a conclusive statement about changing provenance. The XRD results for clay-sized fractions also do not implicate a single dominant source. There are a few relatively clay-rich samples (>20% clay) in Units B and C (4.30, 6.20, 7.00, 7.70 and 8.90 mbsf). In Unit C, only the 8.90 mbsf sample shows mineral abundances different from the unit average. Smectite is 2.5 times more abundant in this sample, at the expense of the non-clay minerals (quartz, calcite and dolomite). The increase in smectite and chlorite content suggest igneous and metamorphic sources for these muds. Local rivers along the coast of Thrace are likely sources for smectite based on the presence of mafic igneous and meta-igneous rocks (e.g., amphibolite) in the hinterland (Bayhan et al., 2005; Natal'in et al., 2012; Bedi et al., 2013).

The only case for which unit averages and their standard deviations for clay-sized components do not overlap is an upcore increase in illite abundance. The illite/smectite ratio has been proposed as a tracer for source areas in the Black Sea (Hay, 1987), with a Danube ratio of ~5 and ratios ~1 or less from Anatolian sources. The illite/smectite ratio for the five Danube samples analysed for this paper is 1.83. The average ratio for MAR02-45 samples is 2.85, and for Unit C is 2.46. These ratios are interpreted to rule out Anatolia as a source; however, there is insufficient data on the mineralogy of clay-sized detritus from northern Thrace to exclude some supply from local rivers near the MAR02-45 site. Although a single source cannot be identified with the data available, neither is there evidence for a change in provenance from ~10.3 cal ka to the present.

The provenance implications of the silt- and clay-sized calcite and more minor dolomite remain uncertain. Five standard smear slides were prepared from <62 μm fractions at 140, 460, 710, 810 and 910 cm composite depths in core MAR02-45 (Fig. 2A). In the two deepest samples, a few strongly recrystallized juvenile planktonic foraminifera are present, but otherwise all of the calcite in the five samples consists of angular, clear monocrystalline particles with no biogenic textures or fabrics. In the uppermost smear slide from Unit A, no coccoliths could be found even though *Emiliania huxleyi* migrated into the Black Sea at ~2.7 cal ka (Jones and Gagnon, 1994). There is a striking similarity between the occurrence of silt-sized calcite described here and the silt-sized calcite described by Major et al. (2002) from cores collected on the Romanian slope outboard of the Danube Delta, except that they describe the calcite as euhedral crystals. Major et al. (2002) indicate an abundance of >60% silt-sized calcite in sediment with an age of ~11–9.1 cal ka.

There are no calcareous algae (e.g., Charaphycean algae) or indigenous calcareous dinoflagellates living in the modern Black Sea that might account for 10–30% calcite in the MAR02-45 succession. Planktonic foraminifera do not live in the Black Sea today, and were last present as juvenile immigrants during the Eemian (Marine Isotopic Stage 5e; Quan et al., 2013). As argued above for rare, long-spined specimens of *Lingulodinium machaerophorum*, the planktonic foraminfera suggest minor recycling of older Pleistocene detritus into the basal part of Unit C. It is hypothesized that the calcite and minor dolomite might be detritus from carbonate bedrock or from calcareous loess in river watersheds, which can contain as much as 40% carbonate – both calcite and dolomite – with the calcite formed mainly by pedogenetic processes (Smalley and Leach, 1978; Újvári et al., 2010). Major et al. (2002) interpreted silt-sized calcite of essentially the same age as an inorganic precipitate formed under evaporative conditions during the early Holocene. The absence of euhedral crystals in the MAR02-45 smear slides does not support this type of interpretation for sediments on the southwestern shelf, and the evidence presented in this paper for an early Holocene transgression is inconsistent with evaporative conditions. If the calcite and dolomite were eroded from carbonate rocks, these likely did not include the Eocene–Oligocene limestones of northern Thrace because they are highly fossiliferous (Varol et al., 2009) and detritus would certainly include recognizable fossil fragments.

Within each lithologic unit, strongly cross-correlated chemical elements can serve as proxies for one another. Sc and Fe are correlated at the R ≥ 0.80 level in all units, presumably because Sc, Fe (and Al) are present in clay minerals and other phyllosilicates (Das et al., 1971). Beyond the shelf edge, it has been shown that Co, Ce, La, Th and Y tend to reside in detrital aluminosilicates (Dean and Arthur, 2011). In the MAR02-45 samples, Unit B in particular shows a strong association of four of these five elements with Sc and Fe. Hence, Sc, Fe, Co, Ce, La, Th and Y are considered to have a detrital origin. Ce is included in this list because for the entire core it is closely correlated with Sc, Th and Fe. Sm is closely tied to La in Units A and C, so is believed to have a detrital origin.

V, Ni, Zn and Cu tend to be concentrated in organic-rich Black Sea sediments (Kıratlı and Ergin, 1996; Dean and Arthur, 2011), either because of biogenic fixation or adsorption under reducing conditions in the sediment (i.e., earliest diagenesis). However, in some circumstances V and Ni can be tied to the detrital supply (Dean and Arthur, 2011). Unit B in particular shows a strong cross-correlation of these elements, and K. In Unit C, V, Ni and Zn are correlated with one another, but also with Sc, Fe and K. The partial mingling of elements which are commonly found in detrital components (i.e., Sc, Fe, K, Th) with those known to accumulate from pore water and on organic components is interpreted to indicate adsorption onto fine-grained phyllosilicates during early diagenesis. Hence, it is believed that V, Ni, Zn, Cu and probably Pb cannot be used to track changes in the nature of detrital supply (i.e., provenance). Instead, they are viewed as elements incorporated from seawater and pore water during early diagenesis.

A prominent feature of Unit C is elevated Cr values from 8.0–7.0 mbsf (~9.4 cal ka) that do not correlate with peaks in other elements. Cr is generally attributed to the weathering of mafic or ultramafic source rocks (Kıratlı and Ergin, 1996). This sample depth range is associated with sandy horizons in core MAR02-45 (Fig. 2A). Samples were taken to avoid the sandy layers, but it is possible that bioturbation had introduced Cr into adjacent muds. The sandy horizons have been interpreted as turbidites or tempestites sourced from the nearby coast or rivers in flood (Hiscott et al., 2007a), and the contrast between the chemistry of these mud samples and other parts of Unit C might indicate sediment supply from more than one provenance, one local (i.e., the event beds), and one more distant.

There is a caveat to any geochemical comparison of core samples to modern detritus from potential source areas. Modern and near-surface grab samples are prone to contamination from industrial pollution and agricultural runoff. Cu, Ni, Zn, and As values are known to be influenced by anthropogenic input (Dinescu and Duliu, 2001; Oreščanin et al., 2005). Fe, Co, Mg, Mn and Cr are potentially more reliable source indicators, but even these elements can be industrial pollutants in floodplain soils and surficial marine sediments. Modern palynological samples of microplankton in the outer Danube Delta and offshore may suffer from the same anthropogenic bias but the characteristics of the refractive particulate matter (kerogen) are more robust and typify all large fluvio-deltaic systems (e.g. Yanko-Hombach et al., 2013).

Based on information in the literature and results presented in this paper, it does not seem possible to track the source(s) of Fe, Co, Cu, Sr, Ni, Mg, and Pb. The exception is perhaps Cr, because of its expected derivation from mafic rocks and their presence in the Strandja Massif (synonym = Istranca Massif) of northern Thrace (Natal'in et al., 2012; Bedi et al., 2013).

## 5. Discussion

The geochemistry and mineralogy of Black Sea sediments are examined in many publications (Hirst, 1974; Stoffers and Müller, 1978; Trimonis and Ross, 1978; Hay, 1987; Kıratlı and Ergin, 1996; Major et al., 2002; Bayhan et al., 2005; Dean and Arthur, 2011; Piper and Calvert, 2011), but published work has emphasized the anoxic portions of the basin and previously did not extend into the earliest, pre-reconnection transgressive deposits on the shelf. Before the last transgression, the Black Sea was not an anoxic basin (Deuser, 1974) so processes of metal transport and fixation were different than today. The water column on the modern shelf is oxygenated, although sulphate reduction in surface muds depletes the pore-water oxygen in Unit A (Hiscott et al., 2007a).

The primary aim of this paper has been to assess whether the provenance of the fine fractions (silt and clay) of the Holocene sediments on the southwestern Black Sea shelf might have changed since the earliest Holocene. Hiscott et al. (2007a) have claimed that the middle part of the southwestern shelf was fully open and connected to the deep Black Sea basin, and hence regional sediment sources, since ~10.3 cal ka, whereas Ryan et al. (2003) and Lericolais et al. (2007) maintain that the central Black Sea had a level below the modern shelf edge until ~9.1 cal ka so that earliest Holocene mud deposits on the southwestern shelf would have had to accumulate in a perched coastal lake.

Neither geochemistry nor XRD mineralogy require a different sediment provenance before and after the ~9.1 cal ka reconnection between the Black Sea and the Mediterranean Sea. Although some detritus in the oldest Unit C appears to have come from nearby coastal areas (e.g., Cr-enriched muds associated with very fine sand and coarse silt event beds) or transgressive reworking of the shelf at the $\alpha$ unconformity (e.g., exotic dinoflagellate cysts and rare planktonic foraminifera), the volume of sediment in seismic unit 1B (equivalent to lithologic Unit C) far exceeds the expected yield of local drainage basins even when summed over a 5000 year interval. Holocene muds of equal or greater thickness along parts of the Bulgarian coast (Dimitrov et al., 1998) than those surrounding core sites MAR02-45 and MAR05-03, the counterclockwise track of the Rim Current around the margins of the Black Sea (Oğuz and Beşiktepe, 1999; Flood et al., 2009), and the southward direction of longshore currents (Panin and Jipa, 2002) are consistent with the hypothesis that the southwestern shelf was open to the main Black Sea basin since the onset of deposition of Unit C and was receiving a significant supply of sediment from large rivers like the Danube and Kamchiya to the northwest. The silt-dominated texture of the muds at sites MAR02-45, MAR05-03 and MAR05-50 (Flood et al., 2009) raises the possibility that the thick, now extensively dissected loess blanket in the Danube drainage basin (Smalley and Leach, 1978; Haase et al., 2007; Fitzsimmons et al., 2012) might account for a strong flux of silt into the western and southwestern Black Sea during the Holocene. Other authors (Ross and Degens, 1974; Bahr et al., 2005; Piper and Calvert, 2011) have noted a dramatic ~10-fold decrease in sediment delivery from the Danube system to the deep portions of the Black Sea after the last transgression, with the river load instead being advected alongshore (Piper and Calvert, 2011).

New palynological data from the Danube Delta and limans in the northwestern Black Sea (Frail-Gauthier and Mudie, 2014) additionally show that the presence of brackish water dinoflagellate cysts, as in Unit C on the southwestern shelf, is characteristic of mixed fluvial and marine waters like those seaward of the modern delta, as opposed to liman environments where only freshwater dinocysts occur (Table 2). A perched coastal lake would have similar fauna and flora to the freshwater limans of today, distinctly different to the fossil remains found in Unit C. Transport of *Pediastrum*, bisaccate pollen and fern spores down river systems, into the marine environment, and then long distances from the points of fluvial input is a well-known phenomenon (Yanko-Hombach et al., 2013) that easily explains the presence of these components in Unit C at the MAR02-45 core site. Our palynological data are generally consistent with the paleome (genetic marker) data of Coolen et al. (2013, their Unit C1 in a core from the Danube Delta slope at −971 m rmsl) but indicate a greater amount of terrigenous material on the shelf at site MAR02-45 than at the deep water site of those authors.

Potentially surprising features of the clay mineralogy are fluctuations by a factor of ~2–3× in smectite abundance throughout core MAR02-45, one major spike in smectite abundance in Unit C, and some large swings in kaolinite abundance in Unit B (Fig. 2E). If the bulk of the mud was derived from distant sources, as hypothesized, then why would the composition not be more uniform? There are a few possible explanations. First, the <2 μm fraction is actually quite small (Fig. 2B) and, on average, ~45% of that size fraction is quartz and carbonate minerals, so that a minor additional amount of one clay mineral can rapidly skew the proportions of the other three clays. This could be the case for smectite, since it has been argued that sandy and silty event beds in Unit C likely were derived from coastal Thrace where smectite is likely more prevalent than in northern sources, based on the presence of mafic igneous and meta-igneous rocks in Thrace (Natal'in et al., 2012; Bedi et al., 2013). Secondly, it is well known that there is a grain-size influence on clay mineral content, so that higher relative amounts of kaolinite in Unit B might simply reflect the coarser texture at this level (Fig. 2B, E), since kaolinite crystallites tend to be larger than those of other clay minerals (Gibbs, 1977). Thirdly, it is to be expected that floods in one drainage basin (e.g., Kamchiya River) or heavy rainfall or spring melt in one tributary of the Danube River could introduce a pulse of sediment having a composition somewhat different to the core average. Alternative, storms might introduce small but variable amounts of material from local sources to modify the bulk clay mineral composition. Finally, all clay mineral analyses are to some extent semi-quantitative. Downcore plots in the studies listed in Table 1 show sample-to-sample fluctuations similar to those in Fig. 2E. Some of this variability must be ascribed to slight inaccuracies and imprecision inherent in the XRD method, and must be taken into account during interpretation of the data.

## 6. Conclusions

There are three strong arguments for an unimpeded connection of a transgressed southwestern shelf to the open Black Sea since at least 10.3 cal ka and perhaps as early as ~12 cal ka.

1) There is a serious discrepancy between the volume (or mass) of sediment available from local small rivers of northwestern Turkey and the actual amount of sediment forming seismic unit 1B (= lithologic Unit C). For sources outside the immediate area to have contributed a majority of the sediment, the southwestern shelf would need to have been accessible to major currents capable of advecting sediment from larger rivers, and to significant wind fetches to periodically redistribute sediment from coastal areas and the transgressive unconformity, $\alpha$.
2) There is a lack of significant mineralogical variation from the early Holocene to the present day in core MAR02-45, which implies that the predominant highstand sources today, the Danube River and perhaps the Kamchiya River, were delivering detritus to the core site since at least 10.3 cal ka.
3) Sc, Fe, Co, Ce, La, Th and Y, interpreted to represent the contribution of aluminosilicates from a terrestrial source, show no significant upcore variation that might suggest a switch from local to regional sources at the time of reconnection of the Black Sea to the world ocean. Instead, continuity in the composition of the detrital supply is indicated.

These points do not rule out a contribution to Unit C from northwestern Turkey (i.e., Thrace). However, this contribution appears to have been small. It is largely masked by a more voluminous regional supply, but is inferred from Cr peaks associated with storm events that affected coastal areas, from a small number of reworked older palynomorphs and planktonic foraminifera that were derived either from coastal erosion or transgressive reworking of the formerly exposed shelf, and from fluctuations in smectite content.

Other researchers have questioned the persistence of a low Black Sea level until ~9.1 cal ka as advocated by Ryan et al. (2003), Ryan (2007) and others. This paper adds weight to the view that the Black Sea rose by increased riverine inflow centuries to millennia before the initiation of water exchange with the Mediterranean Sea through the Bosphorus Strait. The consequences of a much earlier rise in water level must be considered by archeologists concerned with human adaptation in the region, paleoceanographers investigating the development of basin-wide anoxia, paleoclimatologists wishing to explain increased early Holocene precipitation over watersheds leading to the Black Sea basin and the impact of basin-wide anoxia on global carbon budgets, and researchers working in the Marmara and Aegean seas, which might have experienced earlier Black Sea outflow than previously thought.

## Acknowledgments

The authors thank the officers, crew and scientific staff of the R/V *Koca Piri Reis* for their assistance in data acquisition. Lister thanks Memorial University of Newfoundland for the award of a graduate fellowship. Aksu, Hiscott and Mudie acknowledge research grants (RGPIN42760, RGPIN6088, and RGPIN55408, respectively) and ship-time grants (RGPIN228436, RGPIN250825 and RGPIN313115) from the Natural Sciences and Engineering Research Council of Canada (NSERC). H. Gillespie and W. Aylward are thanked for assistance with sediment preparation, palynology processing, magnetic susceptibility measurements and XRD analysis. Drs. G. Oaie and D. Jipa (Romania) are thanked for providing five surficial sediment samples from the Danube Delta; Prof. Valentina Yanko-Hombach (Ukraine) kindly provided Danube prodelta samples for palynology studies. Colleague Dr. Joe Macquaker first alerted the authors to the possibility that erosion of central European loess might account for the predominance of silt on the SW Black Sea shelf.

## References

ActLabs, 2010. 2010 Canadian schedule of services and fees. http://www.actlabs.com (p. 1–32).

Aksu, A.E., Hiscott, R.N., Yaşar, D., Işler, F.I., Marsh, S., 2002. Seismic stratigraphy of Late Quaternary deposits from the southwestern Black Sea shelf: evidence for noncatastrophic variations in sea-level during the last 10,000 Years. Marine Geology 190, 61–94.

Bahr, A., Lamy, F., Arz, H., Kuhlmann, H., Wefer, G., 2005. Late Glacial to Holocene climate and sedimentation history in the NW Black Sea. Marine Geology 214, 309–322.

Ballard, R.D., Coleman, D.F., Rosenberg, G.D., 2000. Further evidence of abrupt Holocene drowning of the Black Sea shelf. Marine Geology 170, 253–261.

Baltes, N., 1971. Pliocene dinoflagellata and acritarcha in Romania. In: Farinacci, A. (Ed.), Proceedings of the 2nd Planktonic Conference, Rome, 1970. Edizioni Tecnoscienza, Rome, Italy, pp. 1–16 (plates 1–5).

Bayhan, E., Ergin, M., Temel, A., Keskin, S., 2005. Mineralogy of Holocene sediments from the southwestern Black Sea shelf (Turkey) in relation to arovenance, sea-level and current regimes. Journal of the Geological Society of China 79, 552–563.

Bedi, Y., Vasilev, E., Dabovski, C., Ergen, A., Okuyucu, C., Doğan, A., Tekin, K., Ivanova, D., Boncheva, I., Lakova, I., Sachanski, V., Kuşçu, I., Tuncay, E., Demiray, G.D., Soycan, H., Göncüoğlu, M., 2013. New age data from tectonostratigraphic units of the Istranca "Massif" in NW Turkey: a correlation with SE Bulgaria. Geologica Carpathia 64, 255–277.

Biscaye, P.E., 1964. Distinction between kaolinite and chlorite in recent sediments. American Mineralogist 49, 1282–1289.

Biscaye, P.E., 1965. Mineralogy and sedimentation of recent deep-sea clay in the Atlantic Ocean and adjacent seas and oceans. Geological Society of America Bulletin 76, 803–832.

Carozza, J.-M., Micu, C., Mihail, F., Carozza, L., 2012. Landscape change and archaeological settlements in the lower Danube valley and delta from early Neolithic to Chalcolithic time: a review. Quaternary International 261, 21–31.

Coolen, M.J.L., Orsi, W.D., Balkema, C., Quince, C., Harris, K., Sylva, S.P., Filipova-Marinov, M., Giosan, L., 2013. Evolution of the plankton paleome in the Black Sea from the deglacial to anthropocene. Proceedings of the National Academy of Science 110, 8609–8614.

Das, H.A., Zonderhuis, J., van der Marel, H.W., 1971. Scandium in rocks, minerals and sediments and its relation to iron and aluminum. Contributions to Mineralogy and Petrology 32, 213–244.

Dean, W.E., Arthur, M.A., 2011. Geochemical characteristics of Holocene laminated sapropel (Unit II) and underlying lacustrine Unit III in the Black Sea. United States Geological Survey Open-File Report 2010-1323, pp. 1–29.

Deuser, W.G., 1974. Evolution of anoxic conditions in Black Sea during Holocene. In: Degens, E.T., Ross, D.A. (Eds.), The Black Sea — Geology, Chemistry, and Biology. American Association of Petroleum Geologists Memoir 20, pp. 133–136.

Dimitrov, P., Michova, E., Peytchev, V., 1998. Palaeoecological reconstructions of western part of the Black Sea during the Quaternary. Proceedings of the Institute of Oceanology 2, 127–139 (in Bulgarian with English summary).

Dinescu, L.C., Duliu, O.G., 2001. Heavy metal pollution of some Danube Delta sediments studied by neutron activation analysis. Applied Radiation and Isotopes 54, 853–859.

EIE, 1991. Water Year Discharges, Elektrik İşleri Etüd İdaresi Genel Müdürlüğü. Ankara, Turkey.

Evans, J.M., 2004. Noah's Flood: fact or fiction? A palaeoenvironmental study of Holocene Black Sea ostracoda. M.Sc. Micropalaeontology project report. University College, London, UK.

Filipova-Marinova, M., Christova, R., Bozilova, E., 2004. Palaeoecological conditions in the Bulgarian Black Sea area during the Quaternary. Environmental Micropaleontology, Microbiology and Meiobenthology 1, 136–154.

Fitzsimmons, K.E., Marković, S.B., Hambach, U., 2012. Pleistocene environmental dynamics recorded in the loess of the middle and lower Danube basin. Quaternary Science Reviews 41, 104–118.

Flood, R.D., Hiscott, R.N., Aksu, A.E., 2009. Morphology and evolution of an anastomosed channel network where saline underflow enters the Black Sea. Sedimentology 56, 807–839.

Frail-Gauthier, J., Mudie, P.J., 2014. Laboratory mesocosms and geological studies for monitoring wetlands diversity. Proceedings of the 2nd Annual Conference on Water Resources and Wetlands, Tulcea (Romania) Sept. 11–13, 2014, pp. 391–403.

Gibbs, R.J., 1965. Error due to segregation in quantitative clay mineral X-ray diffraction mounting techniques. American Mineralogist 50, 741–751.

Gibbs, R.J., 1977. Clay mineral segregation in the marine environment. Journal of Sedimentary Petrology 42, 237–243.

Ginzburg, A.I., Kostianoy, A.G., Nezlin, N.P., Soloviev, D.M., Stanichny, S.V., 2002. Anticyclonic eddies in the northwestern Black Sea. Journal of Marine Systems 32, 91–106.

Giosan, L., Donnelly, J.P., Constantinescu, S., Filip, F., Ovejanu, I., Vespremeanu-Stroe, A., Vespremeanu, E., Duller, G.A.T., 2006. Young Danube delta documents stable Black Sea level since the middle Holocene: morphodynamic, paleogeographic, and archaeological implications. Geology 34, 757–760.

Giosan, L., Filip, F., Constatinescu, S., 2009. Was the Black Sea catastrophically flooded in the Early Holocene? Quaternary Science Reviews 28, 1–6.

Gulin, S.B., Artemov, Y.G., Egorov, V.N., Evtushenko, D.B., 2013. The Dnepr Canyon: evidence for a continuous submarine channel link between the outer shelf and the deep-sea basin of the northwestern Black Sea. Geo-Marine Letters 33, 319–324.

Haase, D., Fink, J., Haase, G., Ruske, R., Pécsi, M., Richter, H., Altermann, M., Jäger, K.-D., 2007. Loess in Europe — its spatial distribution based on a European loess map, scale 1:2,500,000. Quaternary Science Reviews 26, 1301–1312.

Hay, B.J., 1987. Particle Flux in the western Black Sea in the Present and over the last 5,000 years: temporal variability, sources, transport mechanisms. Ph.D. Thesis Cornell University, Ithaca, NY.

Hirst, D.M., 1974. Geochemistry of sediments from eleven Black Sea cores. In: Degens, E.T., Ross, D.A. (Eds.), The Black Sea — Geology, Chemistry, and Biology. American Association of Petroleum Geologists Memoir 20, pp. 430–455.

Hiscott, R.N., Aksu, A.E., 2002. Late Quaternary history of the Marmara Sea and Black Sea from high-resolution seismic and gravity-core studies. Marine Geology 190, 261–282.

Hiscott, R.N., Aksu, A.E., Mudie, P.J., Marret, F., Abrajano, T., Kaminski, M.A., Evans, J., Çakıroğlu, A.I., Yaşar, D., 2007a. A gradual drowning of the southwestern Black Sea shelf: evidence for a progressive rather than abrupt Holocene reconnection with the eastern Mediterranean Sea through the Marmara Sea Gateway. Quaternary International 167–168, 19–34.

Hiscott, R.N., Aksu, A.E., Mudie, P.J., Kaminski, M., Abrajano, T., Yaşar, D., Rochon, A., 2007b. The Marmara Sea Gateway since ~16 ka: non-catastrophic causes of paleoceanographic events in the Black Sea at 8.4 ka and 7.15 ka. In: Yanko-Hombach, V., Gilbert, A.S., Panin, N., Dolukhanov, P.M. (Eds.), The Black Sea Flood Question: Changes in Coastline, Climate and Human Settlement. Springer, Dordrecht, pp. 89–117.

Hiscott, R.N., Aksu, A.E., Mudie, P.J., Marret, F., Abrajano, T., Kaminski, M.A., Evans, J., Çakıroğlu, A.I., Yaşar, D., 2010. Corrigendum to "A gradual drowning of the southwestern Black Sea shelf: evidence for a progressive rather than abrupt Holocene reconnection with the eastern Mediterranean Sea through the Marmara Sea Gateway" [Quaternary International, 167–168 (2007) 19–34]. Quaternary International 226, 160.

Jaoshvili, S., 2002. Rivers of the Black Sea. European Environment Agency Technical Report 71.

Jones, G.A., Gagnon, A.R., 1994. Radiocarbon chronology of Black Sea sediments. Deep-Sea Research Part I 41, 531–557.

Kıratlı, N., Ergin, M., 1996. Partitioning of heavy metals in the surface Black Sea sediments. Applied Geochemistry 11, 775–788.

Lericolais, G., Popescu, I., Guichard, F., Popescu, S.M., 2007. A Black Sea lowstand at 8500 yr B.P. indicated by a relict coastal dune system at a depth of 90 m below sea level. In: Harff, J., Hay, W.W., Tetzlaff, D.M. (Eds.), Coastline Changes: Interrelation of Climate and Geological ProcessesGeological Society of America Special Paper. 426. Allen Press Inc., pp. 171–188.

Lericolais, G., Bourget, J., Popescu, I., Jermannaud, P., Mulder, T., Jorry, S., Panin, N., 2012. Late Quaternary deep-sea sedimentation in the western Black Sea: new insights from recent coring and seismic data in the deep basin. Global and Planetary Change 103, 232–247.
Lister, C.J., 2014. Compositional trends through the Holocene mud succession of the southwestern Black Sea shelf, and implications for sedimentary provenance and water-level history. M.Sc. Thesis Memorial University of Newfoundland, St. John's, Canada.
Liu, J.P., Xue, Z., Ross, K., Wang, H.J., Yang, Z.S., Li, A.C., Gao, S., 2009. Fate of sediments delivered to the sea by Asian large rivers: long-distance transport and formation of remote alongshore clinothems. The Sedimentary Record 7 (4), 4–9.
Major, C., Ryan, W., Lericolais, G., Hajdas, I., 2002. Constraints on Black Sea outflow to the Sea of Marmara during the last glacial–interglacial transition. Marine Geology 190, 19–34.
Marret, F., Mudie, P., Aksu, A., Hiscott, R.N., 2009. A Holocene dinocyst record of a two-step transformation of the Neoeuxinian brackish water lake into the Black Sea. Quaternary International 193, 72–86.
Mertens, K.N., Bradley, L.R., Takano, Y., Mudie, P.J., Marret, F., Aksu, A.E., Hiscott, R.N., Verleye, T.J., Mousing, E.A., Smyrnova, L.L., Bagheri, S., Mansor, M., Pospelova, V., Matsuoka, K., 2012. Quantitative estimation of Holocene surface salinity variation in the Black Sea using dinoflagellate cyst process length. Quaternary Science Reviews 39, 45–59.
Mudie, P.J., Marret, F., Rochon, A., Aksu, A.E., 2010. Non-pollen palynomorphs in the Black Sea corridor. Vegetation History and Archaeobotany 19, 531–544.
Mudie, P.J., Yanko-Hombach, V., Kadurin, S., 2014. The Black Sea dating game and Holocene marine transgression. Open Journal of Marine Science 4, 1–7.
Natal'in, B., Sunal, G., Satir, M., Toraman, E., 2012. Tectonics of the Strandja Massif, NW Turkey: history of a long-lived arc at the northern margin of Paleo-Tethys. Turkish Journal of Earth Sciences 21, 755–798.
Nicholas, W.A., Chivas, A.R., Murray-Wallace, C.V., Fink, D., 2011. Prompt transgression and gradual salinisation by amino acid racemization and radiocarbon dating. Quaternary Science Reviews 30, 3769–3790.
Oğuz, T., Beşiktepe, Ş., 1999. Observations on the Rim Current structure, CIW formation and transport in the western Black Sea. Deep-Sea Research I I-46, 1733–1753.
Oğuz, T., Malanotte-Rizzoli, P., Aubrey, D., 1995. Wind and thermohaline circulation of the Black Sea driven by yearly mean climatological forcing. Journal of Geophysical Research 100, 6845–6863.
Okay, A., 2008. Geology of Turkey: a synopsis. Anschnitt 21, 19–42.
Okay, N., Okay, A.I., 2002. Tectonically induced Quaternary drainage diversion in the northeastern Aegean. Journal of the Geological Society, London 159, 393–399.
Oreščanin, V., Lulić, S., Medunić, G., Mikelić, L., 2005. Granulometric and chemical composition of the Danube River sediments, Batina Village, Croatia. Geologica Croatica 58, 185–194.
Özsoy, E., Latif, M.A., Tuğrul, S., Ünlülata, Ü., 1995. Exchanges with the Mediterranean, fluxes and boundary mixing processes in the Black Sea. In: Briand, F. (Ed.), Mediterranean Tributary Seas. Bulletin de l'Institut Océanographique, CIESME Science Series 1, pp. 1–25.
Panin, N., Jipa, D., 2002. Danube River sediment input and its interaction with the northwestern Black Sea. Estuarine, Coastal and Shelf Science 54, 551–562.
Panin, N., Panin, S., Herz, N., Noakes, J.E., 1983. Radiocarbon dating of Danube delta deposits. Quaternary Research 19, 249–255.
Pérez-Arrieta, L., Tabares-Muñoz, C., 2002. Considerations about the variability of the Bragg's law fulfillment. Revista Mexicana de Fisica 50, 96–98.
Petschick, R., 2000. MacDiff 4.2.2 freeware and manual. http://www.geol-pal.uni-frankfurt.de/Staff/Homepages/Petschick/classicsoftware.html (accessed 19/08/2014).
Piper, D.Z., Calvert, S.E., 2011. Holocene and Late Glacial palaeoceanography and palaeolimnology of the Black Sea: changing sediment provenance and basin hydrography over the past 20,000 years. Geochimica et Cosmochimica Acta 75, 5597–5624.
Popescu, I., Lericolais, G., Panin, N., Wong, H.K., Droz, L., 2001. Late Quaternary channel avulsions on the Danube deep-sea fan, Black Sea. Marine Geology 179, 25–37.
Popescu, I., Lericolais, G., Panin, N., Normand, A., Dinu, C., Le Drezen, E., 2004. The Danube submarine canyon (Black Sea): morphology and sedimentary processes. Marine Geology 206, 249–265.
Quakernaat, J., 1970. Direct diffractometric quantitative analysis of synthetic clay mineral mixtures with molybdenite as orientation-indicator. Journal of Sedimentary Research 40, 506–513.
Quan, T.M., Wright, J.D., Falkowski, P.G., 2013. Co-variation of nitrogen isotopes and redox states through glacial–interglacial cycles in the Black Sea. Geochimica et Cosmochimica Acta 112, 305–320.
Reynolds, R., 2012. Correlation of two sediment cores recovered from the SW Black Sea shelf using carbon and sulfur elemental and isotopic geochemistry: implications for paleoceanographic communication between the Black Sea and eastern Mediterranean Sea during the last 12,000 years. Honours B.Sc. Thesis Memorial University of Newfoundland, St. John's, Canada.
Riedinger, N., Brunner, B., Lin, Y.-S., Voßmeyer, A., Ferdelman, T.G., Jørgensen, B.B., 2010. Methane at the sediment–water transition in Black Sea sediments. Chemical Geology 274, 29–37.
Ross, D.A., Degens, E.T., 1974. Recent Sediments of Black Sea. In: Degens, E.T., Ross, D.A. (Eds.), The Black Sea — Geology, Chemistry, and Biology. American Association of Petroleum Geologists Memoir 20, pp. 183–199.
Royse Jr., C.F., Wadell, J.S., Petersen, L.E., 1971. X-ray determination of calcite–dolomite: an evaluation. Journal of Sedimentary Petrology 41, 483–488.
Ryan, W.B.F., 2007. Status of the Black Sea flood hypothesis. In: Yanko-Hombach, V., Gilbert, A.S., Panin, N., Dolukhanov, P.M. (Eds.), The Black Sea Flood Question: Changes in Coastline, Climate and Human Settlement. Springer, Dordrecht, pp. 63–88.
Ryan, W.B.F., Pitman III, W.C., 1999. Noah's Flood: the New Scientific Discoveries About Events That Changed History. Simon and Schuster, New York.
Ryan, W.B.F., Pitman III, W.C., Major, C.O., Shimkus, K., Moskalenko, V., Jones, J.A., Dimitrov, P., Görür, N., Sakınç, M., Yüce, H., 1997. An abrupt drowning of Black Sea Shelf. Marine Geology 138, 119–126.
Ryan, W.B.F., Major, C.O., Lericolais, G., Goldstein, S., 2003. Catastrophic flooding of the Black Sea. Annual Review of Earth and Planetary Sciences 31, 525–554.
Ryan, W.B.F., Carbotte, S.M., Coplan, J.O., O'Hara, S., Melkonian, A., Arko, R., Weissel, R.A., Ferrini, V., Goodwillie, A., Nitsche, F., Bonczkowski, J., Zemsky, R., 2009. Global multi-resolution topography synthesis. Geochemistry, Geophysics, Geosystems 10, Q03014. http://dx.doi.org/10.1029/2008GC002332.
Shuisky, Y.D., 1982. Limans and liman coasts. In: Schwartz, M. (Ed.), Encyclopedia of Beaches and Coastal Environments, Vol. 15 of the Encyclopedia of Earth Sciences. Hutchinson Ross Publishing Co, Stroudsburg, Pennsylvania, pp. 516–518.
Shumilovskikh, L.S., Marret, F., Fleitmann, D., Arz, H.W., Nowaczyk, N., Behling, H., 2013. Eemian and Holocene sea-surface conditions in the southern Black Sea: organic-walled dinoflagellate cyst record from Core 22-GC3. Marine Micropaleontology 101, 146–160.
Siani, G., Paterne, M., Arnold, M., Bard, E., Métivier, B., Tisnerat, N., Bassinot, F., 2000. Radiocarbon reservoir ages in the Mediterranean Sea and Black Sea. Radiocarbon 42, 271–280.
Sidorchuk, A.Yu., Panin, A.V., Borisova, O.K., 2011. Surface runoff to the Black Sea from the East European Plain during Last Glacial Maximum–Late Glacial time. In: Buynevich, I.V., Yanko-Hombach, V., Gilbert, A.S., Martin, R.E. (Eds.), Geology and Geoarchaeology of the Black Sea Region: Beyond the Flood Hypothesis. Geological Society of America, Special Paper 473, pp. 1–25.
Smalley, I.J., Leach, J.A., 1978. The origin and distribution of the loess in the Danube basin and associated regions of east-central Europe: a review. Sedimentary Geology 21, 1–26.
Soulet, G., Ménot, G., Garreta, V., Rostek, F., Zaragosi, S., Lericolais, G., Bard, E., 2011. Black Sea 'lake' reservoir age evolution since the Last Glacial — hydrologic and climatic implications. Earth and Planetary Science Letters 308, 245–258.
Stoffers, P., Müller, G., 1978. Mineralogy and lithofacies of Black Sea sediments. Initial Reports of the Deep Sea Drilling Project 42, Part 2. U.S. Government Printing Office, Washington, pp. 373–411.
Syvitski, J.P.M., Milliman, J.D., 2007. Geology, geography and humans battle for dominance over the delivery of fluvial sediment to the coastal ocean. Journal of Geology 115, 1–19.
Trimonis, E.S., Ross, D.A., 1978. Mineral composition of coarse-silt fraction of the Black Sea Late Cenozoic sediments. Initial Reports of the Deep Sea Drilling Project 42, Part 2. U.S. Government Printing Office, Washington, pp. 413–426.
Újvári, G., Kovács, J., Varga, G., Raucsik, B., Marković, S., 2010. Dust flux estimates for the last glacial period in east central Europe based on terrestrial records of loess deposits: a review. Quaternary Science Reviews 29, 3157–3166.
Underwood, M.B., Basu, N., Steurer, J., Udas, S., 2003. Normalization factors for semiquantitative X-ray diffraction analysis, with application to DSDP Site 297, Shikoku Basin. Data report. In: Mikada, H., Moore, G.F., Taira, A., Becker, K., Moore, J.C., Klaus, A. (Eds.), Proceedings of the Ocean Drilling Program, Scientific Results 190/196, pp. 1–28.
Varga, G., 2011. Similarities among the Plio–Pleistocene terrestrial aeolian dust deposits in the world and in Hungary. Quaternary International 234, 98–108.
Varol, B., Baykal, M., Ayyıldız, T., 2009. Sedimentological–stratigraphical evaluation of Tertiary carbonates (Sogucak Formation) of Thrace Basin (Bozcaada – Kıyıköy). Mineral Resource Exploration Bulletin 139, 1–15.
Weaver, C.E., 1989. Clays, Muds, and Shales. Developments in Sedimentology 44. Elsevier, Amsterdam.
Winguth, C., Wong, H.K., Panin, N., Dinu, C., Georgescu, P., Ungureanu, G., Krugliakov, V.V., Podshuveit, V., 2000. Upper Quaternary water level history and sedimentation in the northwestern Black Sea. Marine Geology 167, 127–146.
Yanko-Hombach, V., 2007. Controversy over Noah's Flood in the Black Sea: geological and foraminiferal evidence from the shelf. In: Yanko-Hombach, V., Gilbert, A.S., Panin, N., Dolukhanov, P.M. (Eds.), The Black Sea Flood Question: Changes in Coastline, Climate and Human Settlement. Springer, Dordrecht, pp. 149–203.
Yanko-Hombach, V., Mudie, P.J., Kadurin, S., Larchenkov, E., 2013. Holocene marine transgression in the Black Sea: new evidence from the northwestern Black Sea shelf. Quaternary International 345, 100–118.
Yankovsky, A.E., Lemeshko, E.M., Ilyin, Y.P., 2014. The influence of shelfbreak forcing on the alongshelf penetration of the Danube buoyant water, Black sea. Continental Shelf Research 24, 1083–1098.